

Evaluation Report

TILT AND VIBRATION ISOLATION SYSTEM

Submitted to:

NASA/ERC
Cambridge, Mass.

Report Number PPD-E-68-E-10245

14 June 1968

Prepared by

B. Rhodes
B. Rhodes
Senior Staff Specialist

Approved by

E. L. Swainson
E. L. Swainson
Chief,
Test Instrumentation

NORTHROP NORTRONICS
Precision Products Department
Norwood, Massachusetts

ABSTRACT

A test program implemented to evaluate the design feasibility of a precision tilt and angular vibration isolation system to eliminate the effects of ground motions from inertial sensors under test is described. A single-axis model is evaluated as an experimental representation of NASA/ERC's proposed tilt isolation system using gyroscope and accelerometer instruments for control. Inclusion of a Nortronics GI-V7 in the model permits monitoring of performance at high frequencies.

Capability of the model to maintain level to within 0.01 arc-second for long time periods in an urban laboratory environment is demonstrated. Major limitations in system performance are found to be level sensor capability, and gyro wheel hunt and noise.

TABLE OF CONTENTS

ABSTRACT	i
1.0 INTRODUCTION.	1
1.1 Background.	1
1.2 Summary of Results.	2
2.0 TEST SYSTEM DESCRIPTION	4
2.1 Single-Axis Model System	4
2.2 Single-Axis Test System Control Design.	5
2.3 System Calibration	7
2.4 Monitor Gyro Calibration	7
3.0 SYSTEM PERFORMANCE	8
3.1 System Loop Gain, Compensation, and Frequency Response.	8
3.2 Transient Response to Torque	11
3.3 Level Loop Operation	12
3.4 Long-Term Level Stability.	13
3.5 Short-Term Level Stability and Gyro Noise	18
4.0 CONCLUSIONS AND RECOMMENDATIONS FOR FURTHER EFFORT	21
APPENDIX A - Monitor Gyro Calibration	
APPENDIX B - GI-T2-A Characteristics	
APPENDIX C - Summary of Project Activity	
APPENDIX D - Major Equipment Used	

1.0 INTRODUCTION

This report, submitted in partial fulfillment of the requirements of Contract NAS-12-580, describes the evaluation of a precision tilt and vibration isolation system test model at NASA/ERC.

1.1 BACKGROUND

The tilts and angular vibrations that exist in most laboratories introduce errors in the testing of inertial grade gyroscope instruments. To overcome such limitations in the testing of the extremely precise gyroscopes used in the Ships Inertial Navigation System of the Polaris Weapons system, Nortronics Precision Products Department has built an ultra-precision test center in Norwood, Massachusetts. This test facility was constructed by excavating to bedrock at the site and constructing on the bedrock a massive concrete base which was isolated from the building structure. Piers for the ultra-precision test stations were attached to this base. This resulted in a considerable attenuation of both cultural noise and long-term tilts.

This solution could not be applied readily, either to the inertial test facility being constructed by the Guidance Laboratory of the NASA Electronics Research Center in Cambridge, Mass., or at most other inertial test facilities. At the NASA/ERC site, bedrock is a full 90 feet below the surface. Cost of excavation to this depth could be prohibitive. In addition, for the extreme accuracies that will be required for future space and aeronautics applications, even the very small tilts and vibrations that would be found on rock would introduce significant errors. It is also desirable to develop a means for testing high-accuracy inertial sensors at locations having large vibration environments, for example a space vehicle launch facility.

To help resolve these problems, NASA/ERC has been conducting studies on the design of a precision tilt and angular vibration isolation system that makes use of gyroscopes and accelerometers for servomechanism control, combined with conventional high-frequency inertia isolation. NASA Technical Report TR R-281 describes an analytical and experimental feasibility study of the design of this system.

As part of this study a full-scale, single-axis model of the servomechanism portion of the system was constructed at NASA/ERC's temporary inertial sensor test laboratory. A Nortronics GI-V7 gyroscope was loaned to NASA/ERC by the Navy Special Projects Office for use in evaluating the performance of the single-axis platform. Engineering support for this evaluation was provided by Nortronics PPD under Contract NAS 12-580.

The objectives of this contract were:

1. Design and construct fixtures for mounting a GI-V7 gyroscope to the experimental platform.
2. Modify existing GI-V7 test electronics to provide a full frequency angular motion measurement capability.
3. Perform calibration and evaluation tests to evaluate the system performance.
4. Conduct tests to determine the suitability of any other available gyroscopes for control of the system.

1.2 SUMMARY OF RESULTS

1. The system data over an almost continuous run period of 78 days indicates that the stabilized system will maintain the level error signal well within ± 0.01 arc-second.
2. The level error data from the GI-T2 controlled system with improved mounting hardware shows an improvement in stability over the original system (described in NASA Technical Report TR R-281) by a factor of four.
3. The tilt error with respect to "true" level is limited by the accuracy of the level sensor. Typically, a differential error between two Ideal Aerosmith level sensors of approximately 0.1 to 0.2 arc-second was experienced.
4. The level stability of the system at higher frequencies was severely limited by a noise disturbance resulting from control gyro wheel hunt. One contributor, an unstable wheel excitation frequency, was corrected which resulted in a significant reduction of this condition. The reduced level,

however, is still unsatisfactory (approximately 0.06 arc-second peak at a frequency of 2.25 Hz). The mechanism by which the platform control servo appears to be coupled into the gyro wheel spin motor system, thus aggravating this instability, requires further study. Tests show that the Precision Tilt and Vibration Isolation System described in TR-R-281 will require a gyro with very low effective wheel hunt as one of its most important characteristics.

2.0 TEST SYSTEM DESCRIPTION

The mechanical configuration and signal flow are discussed in section 2.1, a detailed loop and electrical schematic description appears in section 2.2. Sections 2.3 and 2.4 present the system and monitor gyro calibration results.

2.1 SINGLE-AXIS MODEL SYSTEM

The main structure consists of a 5-3/4 foot triangular steel weldment pivoted at two points and driven at the third by a modified MIT Micro-motion Drive Assembly. A static load of 2100 pounds was added to the platform to bring the total weight to 3000 pounds. The inertial sensors are mounted on a rigid platform at the driven end of the structure (see figure 2.1.1). The GI-T2 control gyro and the GI-V7 monitor gyro are attached to rigid one-inch aluminum angle brackets using the trunnion clamps and hardware normally associated with these gyros, thus providing the thermal conductivity characteristics which have been established for these units. The level sensors rest on a separate one-inch thick surface plate which is attached to the main structure by three spring-loaded bolts. The purpose of this configuration is to approximate a three-point mounting to prevent possible warpages of the main structure from introducing differential angular variations to the level sensors.

The gyros, which are single-degree-of-freedom floated gyros, are temperature controlled. A standard Mark II SINS heater controller sets the temperature of the GI-V7; the GI-T2 gyro is controlled by a specially-built 60-cycle controller. There is no temperature control of the level sensors or of the ambient temperature under the draft shield which is placed over the entire sensor package.

Figure 2.1.2 illustrates the interconnection of the sensors and the drive motor. Two modes of operation are available, as shown in the illustration: 1) a LEVEL mode and a GYRO mode. In the level mode, the platform is maintained level with respect to the gravity force vector by applying the tilt error signal directly to the leveling servo. In the gyro mode, the leveling servo is controlled by the gyro which senses angular variations with respect to inertial space. (Gyro control alone would not be practical since the platform would follow gyro drift; therefore, long-term level control, in the gyro mode, is provided by the level sensor acting through gyro torquer.) The integrator maintains the platform tilt

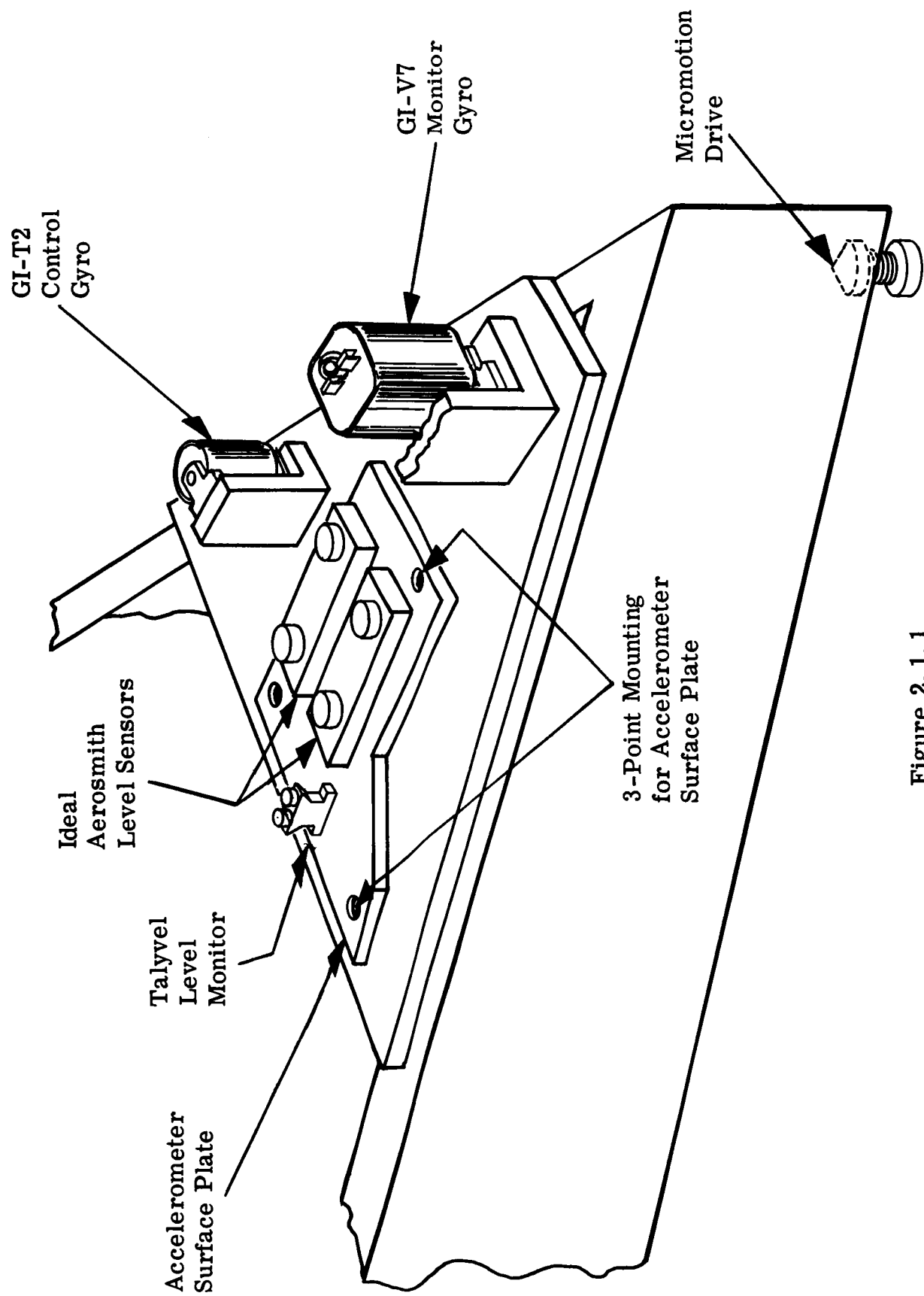


Figure 2. 1. 1

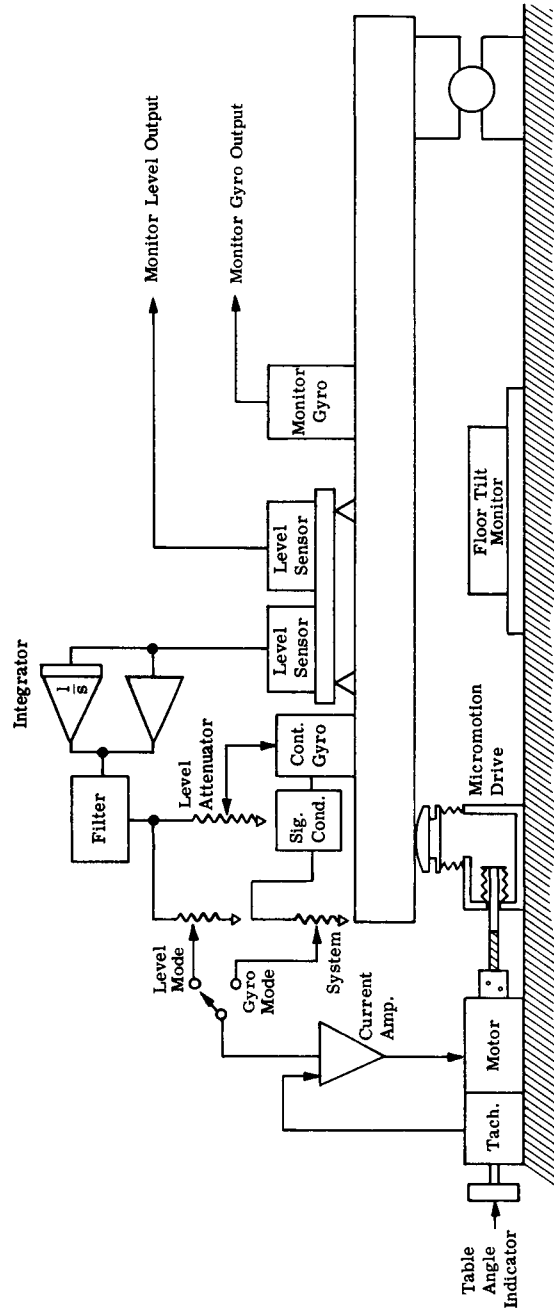


Figure 2.1.2 - Sensor and Drive Motor Interconnections

error at zero in the presence of uncompensated steady-state gyro drift, and at small values during periods of gyro drift ramp. A manually-adjustable circuit for gyro drift compensation is also included. Since the gyro was oriented approximately IA → East, and earth rate input was therefore minimum, this circuit was not particularly critical. In a two-axis system, however, gyro drift correction should be stable to at least 10 parts per million since one of the gyros must see at least 50% of the horizontal component of earth rate.

A Nortronics GI-T2 gas-bearing gyro was made available by the Air Force for use as the control gyro for the system. This gyro, normally used in a north-seeking gyrocompass system, had characteristic parameters sufficiently close to those of the original gyro specified in NASA/ERC TR-R-281 so that it could be adapted to the system with only minor modifications to the loop.

A Nortronics GI-V7 gyro was used for the monitor. This gyro was connected in a low gain capture loop; its microsyn output was amplified, demodulated and calibrated to provide a very sensitive indication of input axis angular variations. The control level was a mercury level type instrument made by Ideal Aerosmith, Inc.; an identical unit was also used for level monitoring. A Taylor-Hobson Talyvel level monitor was also used for some tests. A servo shaft angle indicator on the Micromotion Drive was calibrated to read table angle. For some test runs, a third Ideal Aerosmith tilt sensor was placed underneath the system to read floor tilt.

2.2 SINGLE-AXIS TEST SYSTEM CONTROL DESIGN

A block diagram of the experimental system is shown in figure 2.2.1. This diagram illustrates the three basic loops contained within the system. Gain controls are available in each loop to provide a high degree of flexibility. These basic loops are:

1. System Loop - This loop, which couples the control gyro output to the platform drive motor, provides angular stabilization of the platform to the integrated gyro drift rate angle. A "system gain" control potentiometer in this loop enables a gain adjustment from zero to maximum. System gains throughout this report are specified as decimal fractions of the maximum available open-loop gain. This maximum gain value is computed to be

$$K_{\text{max.}} = 160 \text{ rad./sec.}$$

The principal effect of increasing this gain setting, in addition to increasing loop tightness which reduces gyro (and table) offset angle for a given torque loading, is to increase the upper bandwidth of effective gyro control.

2. Gyro Caging - The gyro caging loop, which couples the gyro output signal back to the gyro torquer, provides a means for setting gyro output axis restraint. The principal effect of varying the gain in this loop is to reduce the lower bandwidth of gyro control. The range of electrical restraint available is from zero to approximately 650 dyne-cm./degree (about OA). Again, gain settings of this loop are reported as decimal fractions of the maximum available gain.
3. Level Loop - The level loop, sometimes referred to as an erection loop, couples the platform to the local (pendulum) vertical. Since this loop also couples horizontal linear acceleration into the platform vertical, it must provide significant filtering of the total accelerometer signal. This loop generates a gyro torquing signal proportional to a constant plus the integral of the accelerometer signal (refer to the Tiltmeter Filter section of figure 2.2.1). In other words, the platform is driven by a rate signal relative to proportional-plus-integral of platform tilt and linear acceleration. Since no steady-state linear acceleration exists, an integrator can be used to provide effectively infinite d-c gain in the level loop to enable the accelerometer signal to go to zero even in the presence of a demand for a gyro drift correction.

Considering only the proportional part of the Tiltmeter Filter network, and ignoring the higher order denominator terms, the closed-loop response of the erection loop (platform angle resulting from linear acceleration) is

$$\frac{\delta(s)}{a(s)} = \frac{\frac{1}{g}}{Ts + 1}$$

$\delta(s)$ = tilt error

$a(s)$ = acceleration

Where: T is a time constant determined by the open-loop gain.

For this particular system, at full gain $T = 0.250$ second and goes to infinity as the level attenuator setting (open loop gain) approaches zero. Thus, the time constant of this loop is materially affected by gain setting. A sharper rolloff at higher frequencies is obtained by the inclusion of filter elements as shown in figure 2.2.1

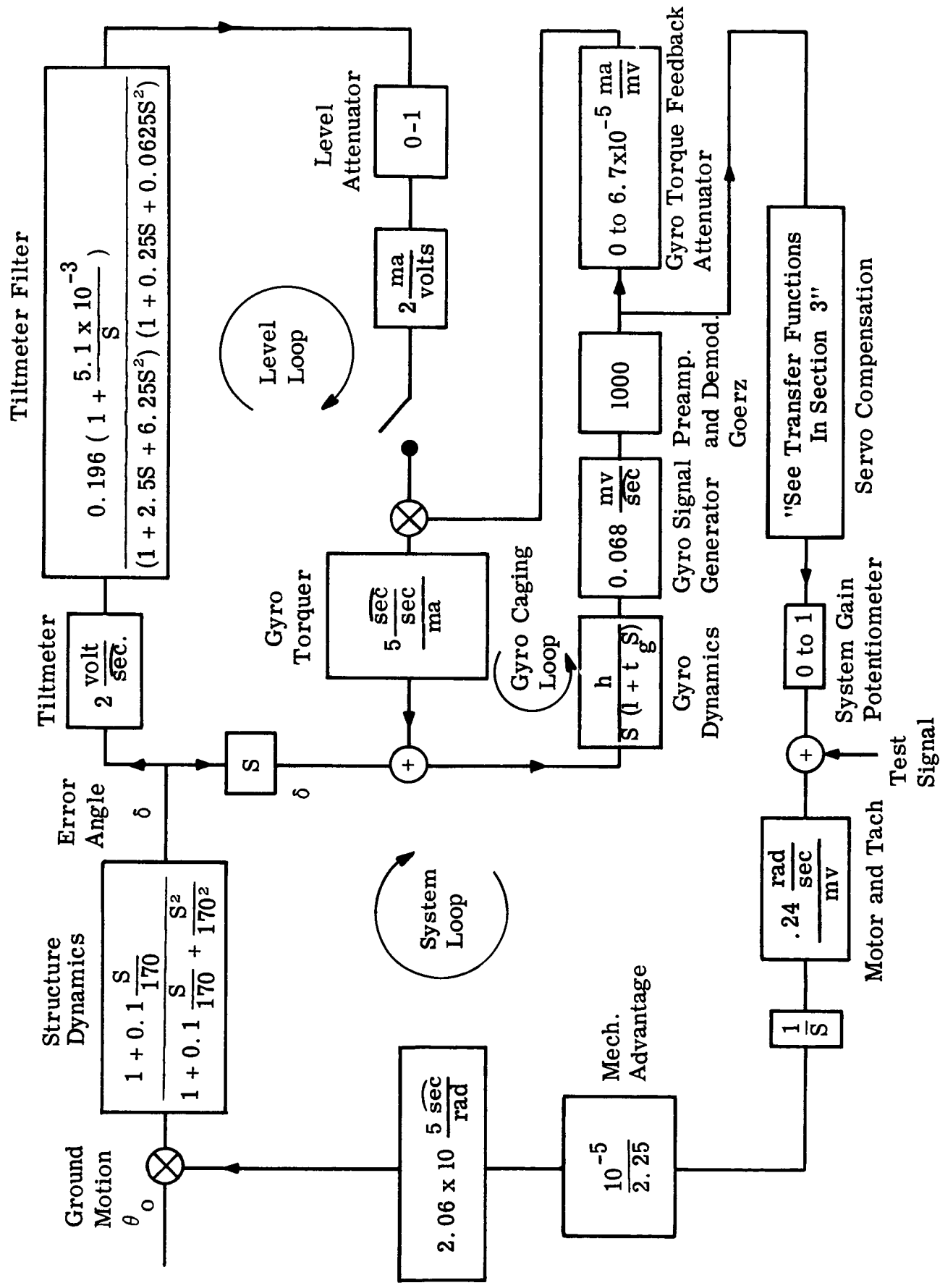


Figure 2.2.1 Block Diagram of Experimental Servomechanism Leveling System

Figure 2.2.2 represents a schematic wiring diagram of the system. A level-control-only mode of operation, not depicted in the previous block diagram, is available by coupling the tilt signal directly through amplifier A13 to the leveling servo. This mode of operation provides a convenient method of comparing gyro and accelerometer loop performance with accelerometer (only) control. Test point 10 at amplifier A12 provides a convenient point for injecting a (velocity) drive signal into the system loop.

2.3 SYSTEM CALIBRATION

A static system calibration was made, utilizing the calibration of the micrometer screws of the Talyvel level sensor for reference.

Calibration was as follows:

Control Level	0.05 arc-sec./div. (meter reading) 0.05 arc-sec./volt (electrical output)
Monitor Level	0.067 arc-sec./div. (meter reading) 0.714 arc-sec./volt (electrical output)
Talyvel	(meter scale direct reading) 0.2 arc-sec./volt (electrical output)

2.4 MONITOR GYRO CALIBRATION

The calibration curve for the GI-V7 monitor gyro is shown in figure 2.4.1. This graph provides a direct conversion from GI-V7 instrument package output voltage to input axis angle as a function of frequency. To correctly interpret angular data, as measured by the monitor gyro, the data must be referred to this curve for calibration at each discrete frequency of interest.

Refer to Appendix A for a discussion of the frequency response of this gyro and the method of obtaining this calibration.

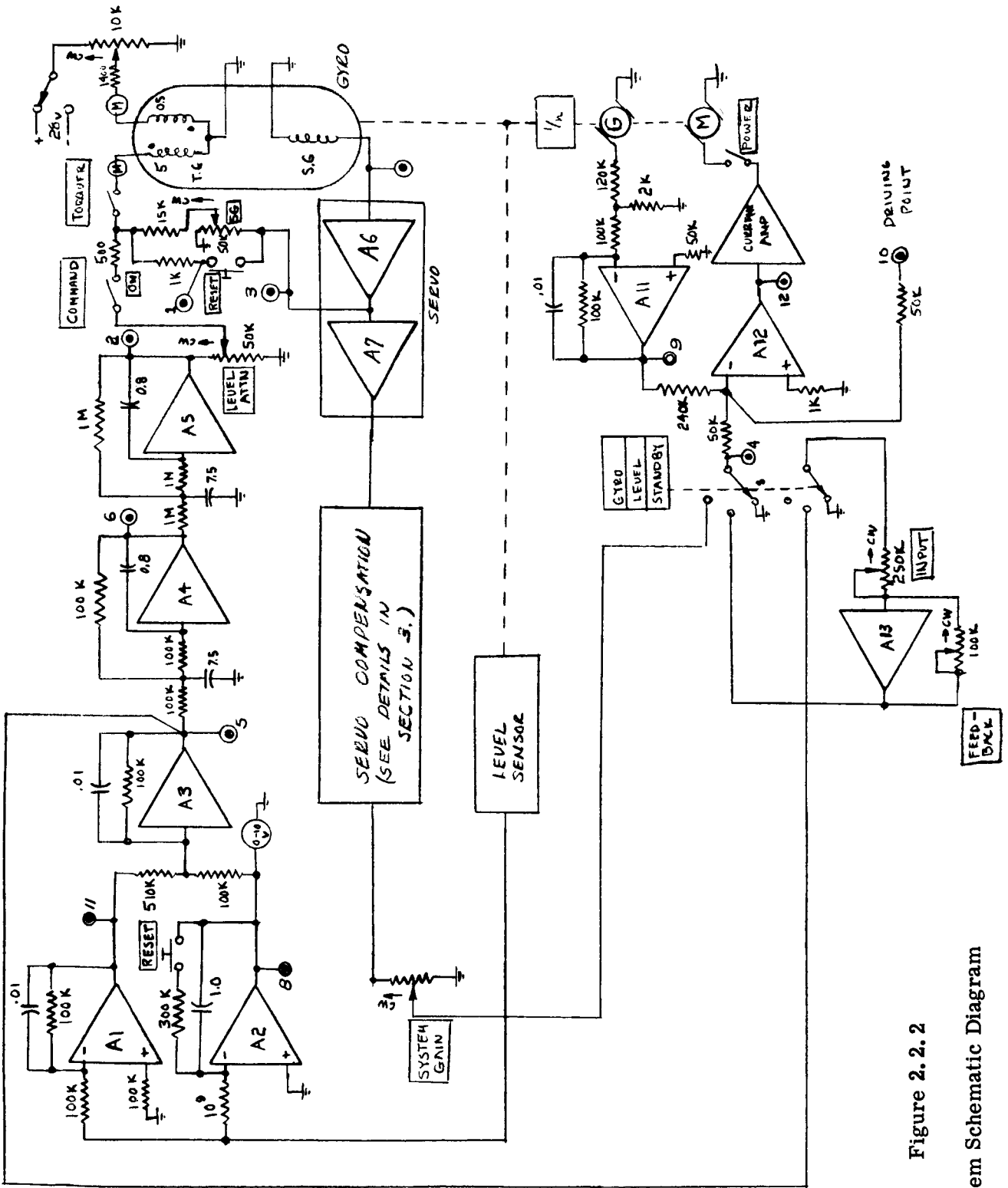
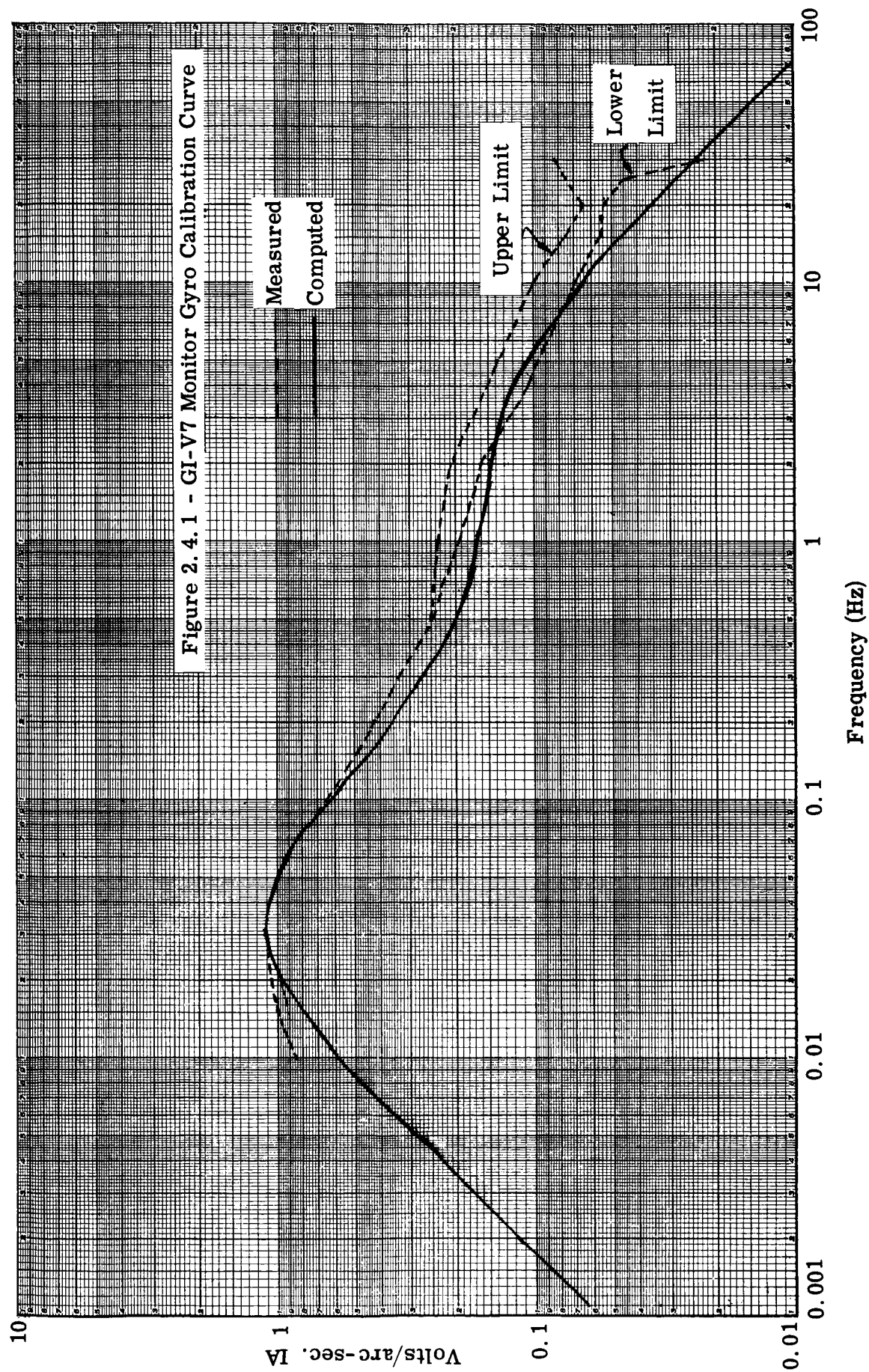


Figure 2.2.2

System Schematic Diagram



3.0 SYSTEM PERFORMANCE

Sections 3.1, 3.2 and 3.3 describe the performance of the System Loop, the Gyro Caging Loop and the Level Loop for various configurations and gain settings.

Section 3.4 presents long-term level stability data and section 3.5 describes short-term stability and gyro noise.

3.1 SYSTEM LOOP GAIN, COMPENSATION, AND FREQUENCY RESPONSE

The object of the following procedure was to determine experimentally a suitable compensation network for the system loop of figure 2.1.1. Due to a 23 Hz mechanical resonance in the system and considerable gyro noise, the various broad bandwidth configurations tried were discarded and a double-lag circuit with a corner frequency of 20 Hz was selected (figure 3.1.8). The closed loop frequency response for this configuration (illustrated in figure 3.1.9) shows an upper bandwidth cutoff beyond 10 Hz.

Although the loop was stable with a gain setting of 0.5 (80 rad./sec.), the system was never run at a gain setting greater than 0.4 because it was discovered that the system could be shocked into a limit cycle oscillation at gain settings greater than this value. While the reason for this phenomenon was not analyzed, saturation of the tachometer amplifier would be the primary suspect due to the very high frequency nature of the noise present; a wheel-hunt condition (described later) could also be a factor.

3.1.1 Procedure

Closed-loop system frequency response was determined by dividing the system (velocity) response voltage measured at Test Point 4 (see figure 2.2.2) by the forcing voltage applied to Test Point 10.

Amplitudes of the output signals below 10 Hz were determined by observing the peak-to-peak deflection of the Brush Recorder traces. Although this instrument itself posed no limitations at any of the frequencies encountered in this experiment, another method was necessary at higher frequencies due to the fact that random excursions (noise) made the recorded data extremely difficult to interpret. A Hewlett Packard Model 3400 True RMS Voltmeter was used to indicate the RMS value of the demodulated GI-V7 output at frequencies above 10 Hz. To be consistent, the RMS data was converted to peak-to-peak values. Good correspondence was obtained at the 10 Hz "crossover point".

The main criterion for selecting the compensation network was to obtain minimum noise and still obtain a reasonable bandwidth. Figure 3.1.13 shows the RMS GI-T2 output axis noise angle plotted against system gain for the four compensation networks tried for the system. Classically, a reduction of the noise (the control servo error signal) should have been observed as the gain was increased; however, this was not the case. The noise and resonant conditions existing at the noise frequencies observed (greater than 20 Hz) were not investigated, but their effect was substantially reduced by resorting to the double-lag compensation circuit of figure 3.1.8. A 2.25 Hz wheel-hunt disturbance, however, which also was part of the noise spectrum measured, is well within the servo bandpass, and makes up the bulk of the noise shown in the minimum noise curve of figure 3.1.13.

3.1.2 Summary of Results

The closed-loop frequency response of the system with compensation as shown in figure 3.1.1 was run on two occasions. It was discovered that the system damping was somewhat higher after the system had been on for several hours, then after about a one-hour warmup. Since the system would normally be in operation almost continuously, the initial data does not represent a realistic condition; however, the data is furnished for information purposes. Figures 3.1.2 and 3.1.3 present a comparison of these two conditions, curve 3.1.3 illustrating the steady-state condition after warmup.

The 0.04 μf feedback capacitor at amplifier A8 was reduced to 0.002 μf , as shown in figure 3.1.4, and the measured closed-loop frequency response for this configuration is shown in figure 3.1.5.

The 23 Hz mechanical resonance which existed in the system was easily observed in the closed-loop response curve of figure 3.1.7 with the system using the simple lag compensation circuit of figure 3.1.6. Figures 3.1.8 and 3.1.9 present the compensation circuit, and its closed-loop response that was ultimately chosen for the system. This configuration produced the lowest noise and a closed-loop bandwidth of about 12 Hz. A Bode analysis (figure 3.1.14) based on the parameters listed in the block diagram, indicates that the system would become unstable as the open-loop gain nears 40 db or 100 rad./sec. The experimental loop became unstable at a gain attenuator setting of 0.5 (equivalent to an open-loop gain of 38 db). The

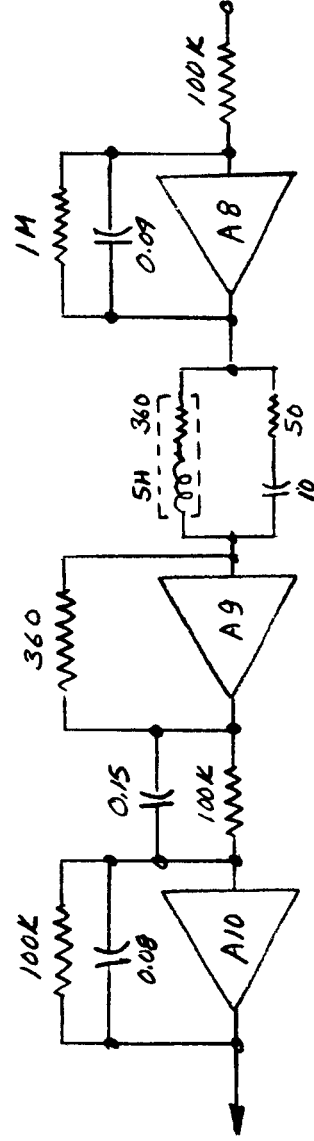
open-loop response of the system could not be measured due to the saturation of the electronics. The closed-loop resonant frequencies were computed from the open-loop parameters taken from the block diagram and they agree fairly well with figure 3.1.9.

Gain	ω_c	ω_c
	Calculated	Measured
0.1	4.9	3.9
0.2	6.75	6.3
0.3	8.4	7.2

Thus, there is experimental verification that the gyro loop block diagram parameters are reasonably representative of the actual system.

Figures 3.1.10 and 3.1.11, when compared with figures 3.1.4 and 3.1.5 respectively, illustrate the effect of removing the 0.015-second lead network. This was tried as another attempt to reduce the high-frequency noise in the system.

Figure 3.1.12 shows the frequency response of the compensation networks used in this experiment.



$$\frac{10(1 + 0.015s)(1 + 0.0045 + \frac{s^2}{140})}{(1 + 0.008s)(1 + 0.9s)(1 + 0.915 + \frac{s^2}{379})^2}$$

Servo Compensation
Figure 3.1.1

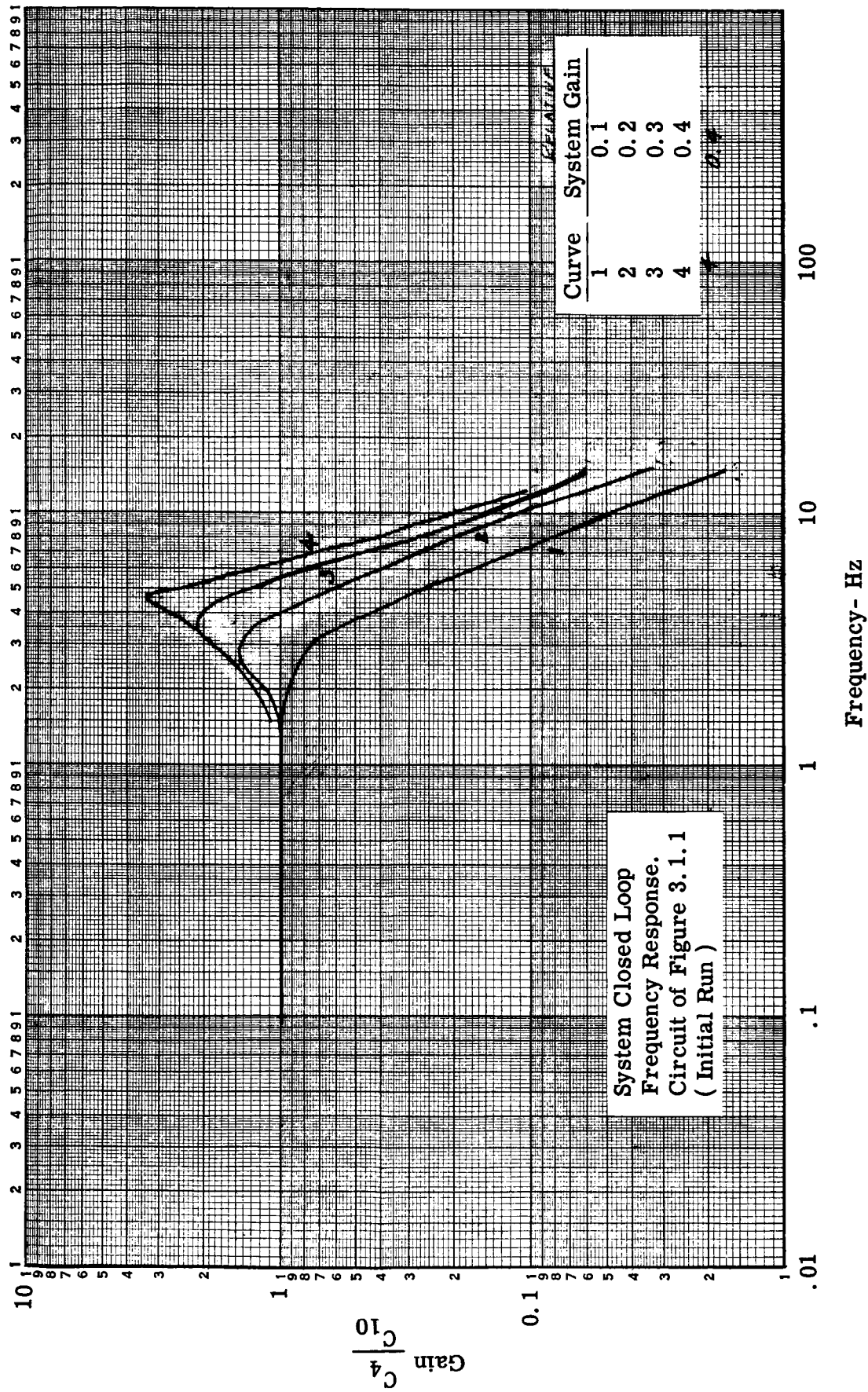
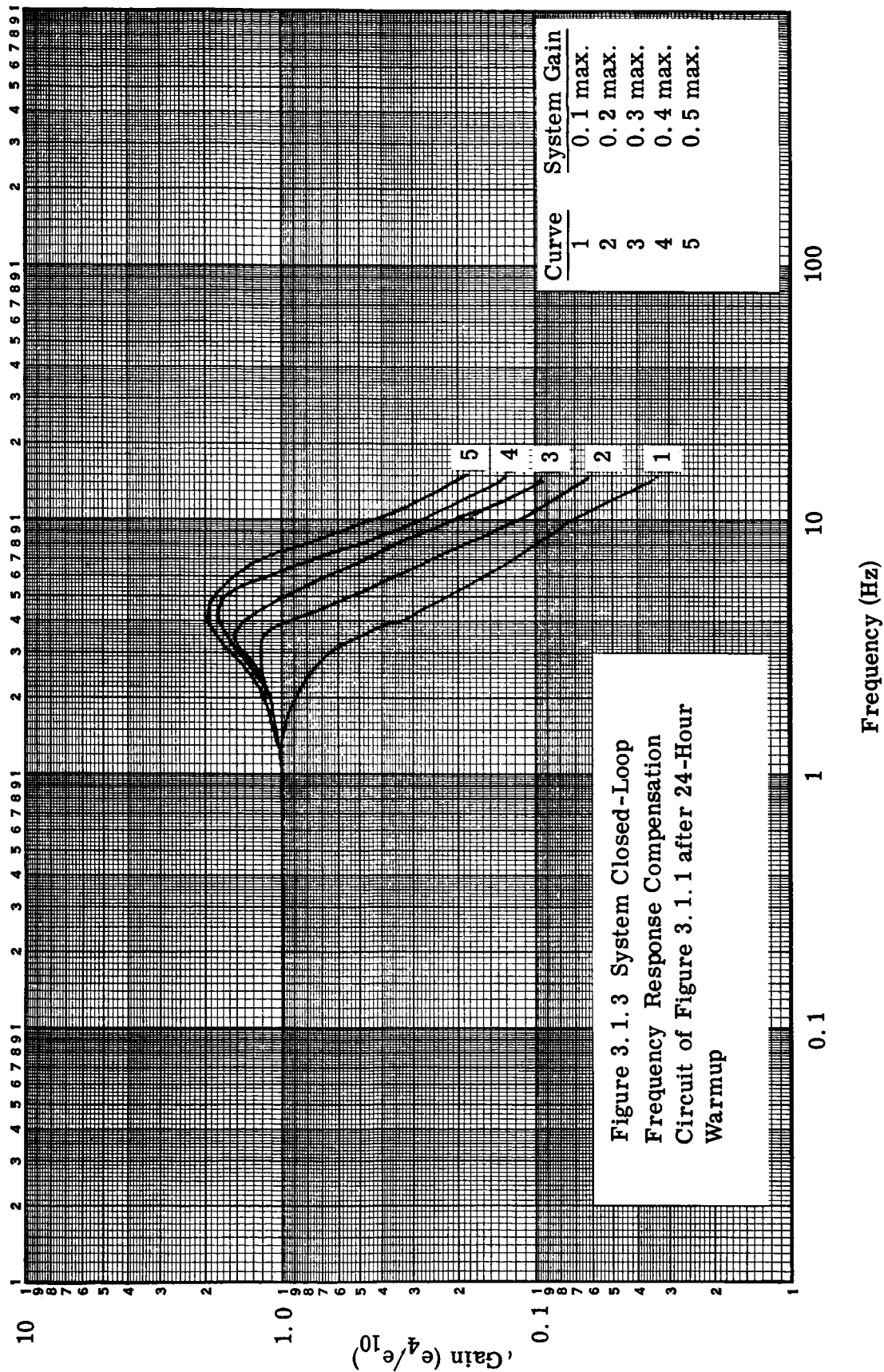
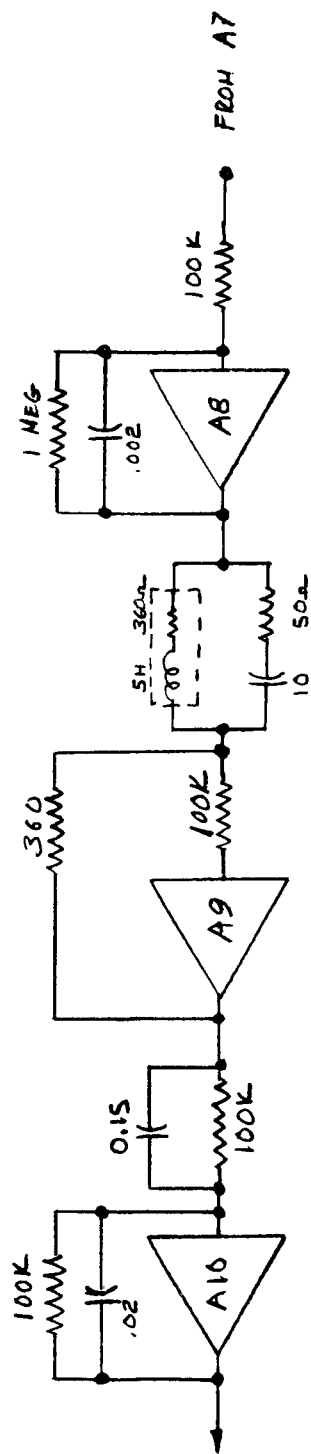


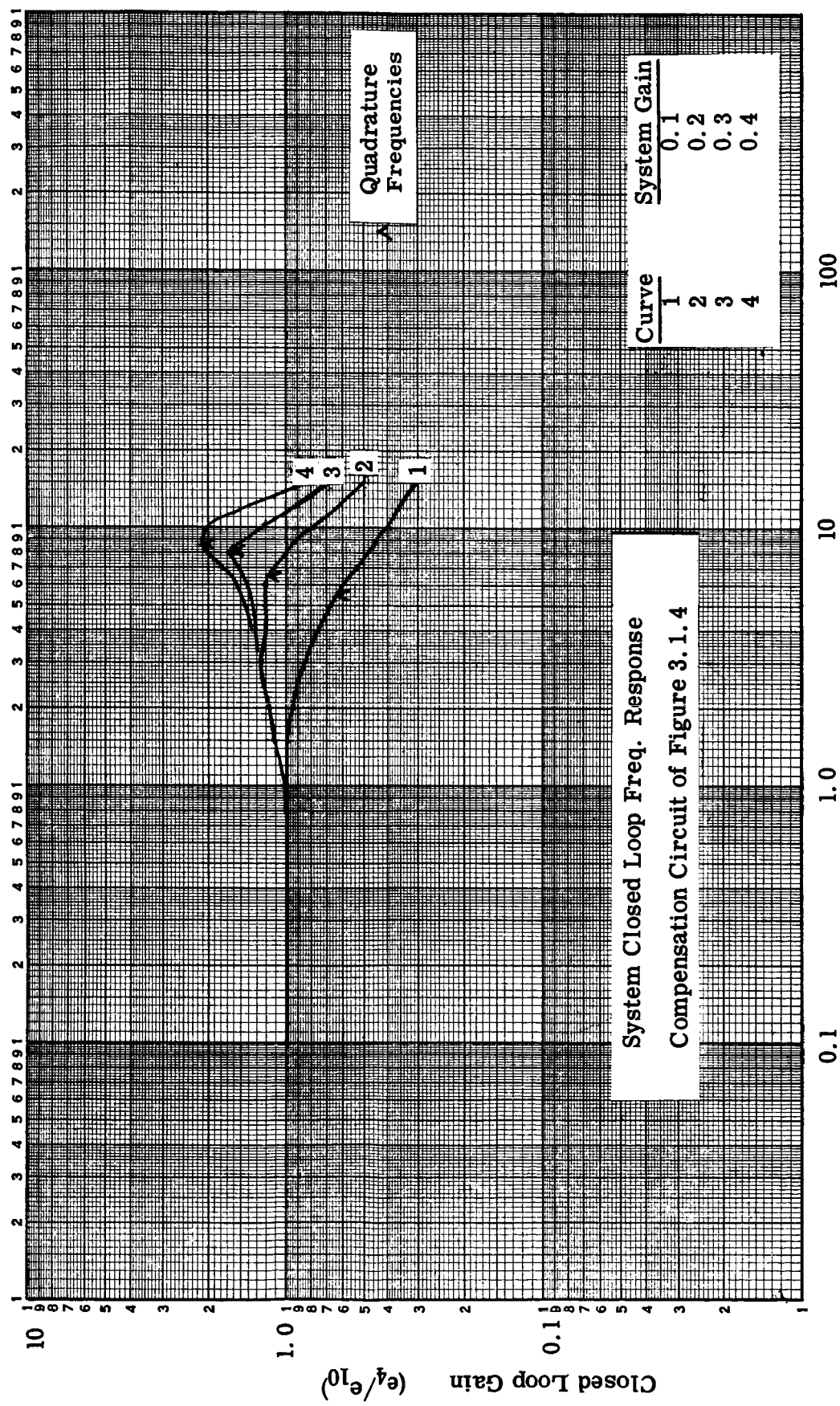
Figure 3.1.2





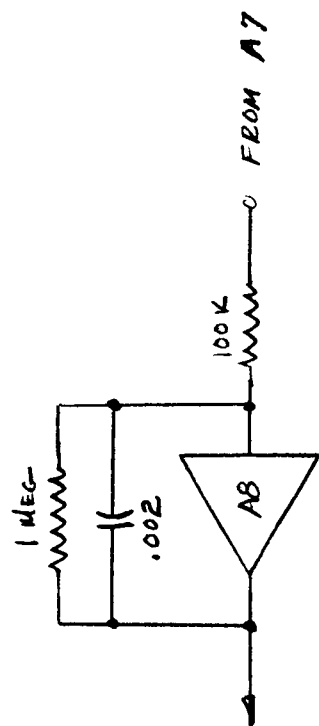
$$\frac{10(1+.015s)(1+.009s + \frac{s^2}{140})}{(1+.002s)^2 (1+.014s + \frac{s^2}{379})}$$

Compensation Network
Figure 3.1.4



Frequency, Hz

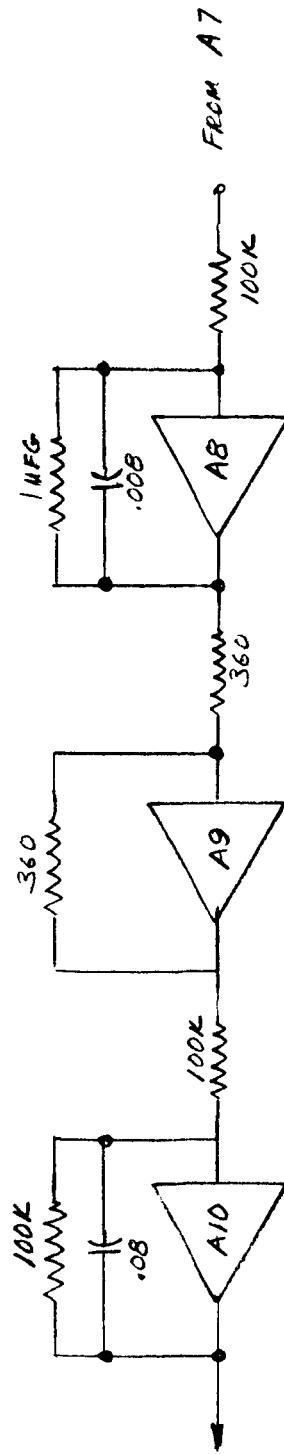
Figure 3.1.5



(A9, A10
AND LG
NETWORK
BY-PASSED)

$$\frac{10}{(1 + .002s)}$$

Figure 3.1.6



$$\frac{10}{(1 + .008s)^2}$$

Compensation Network
Figure 3.1.8

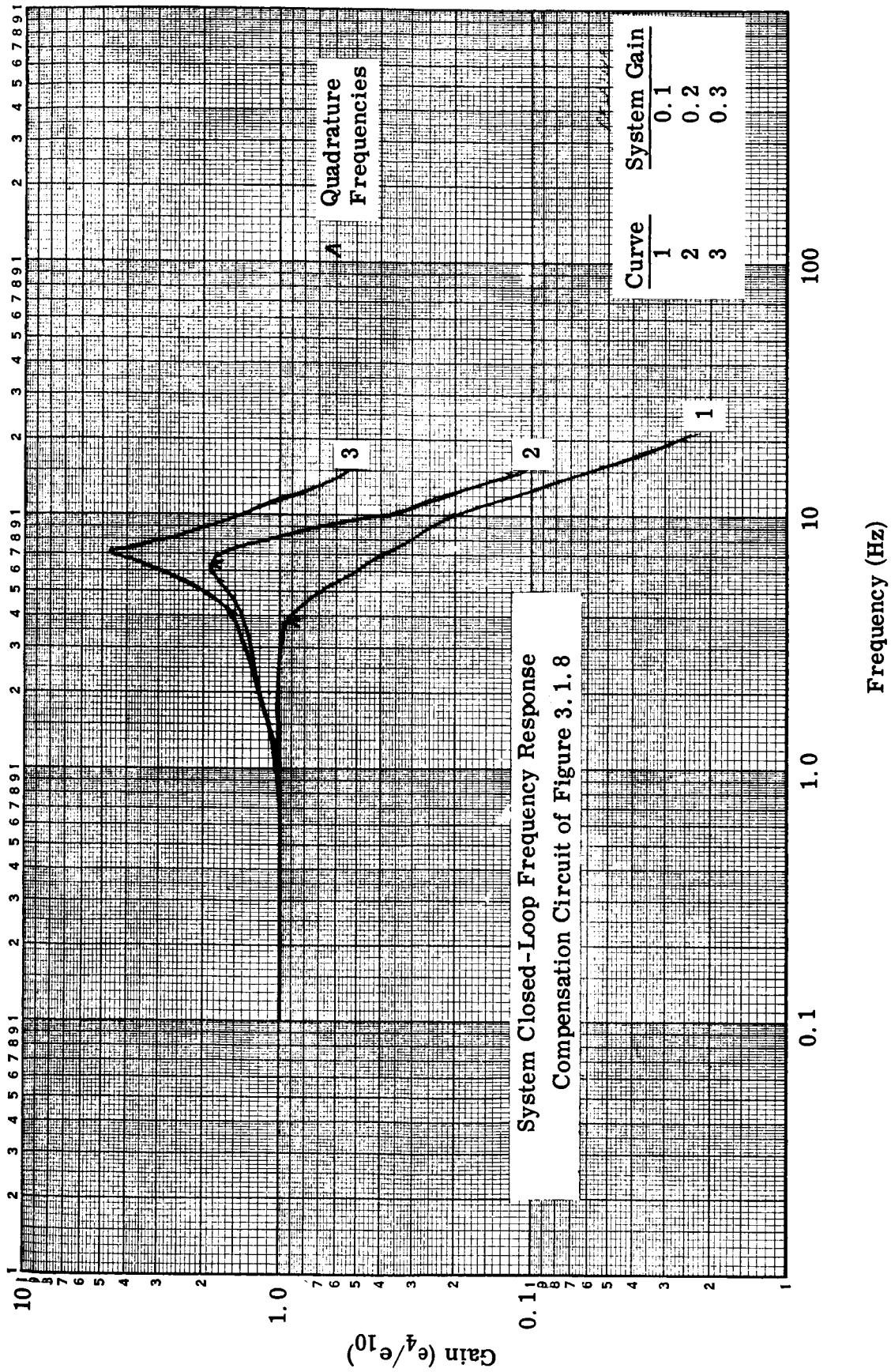
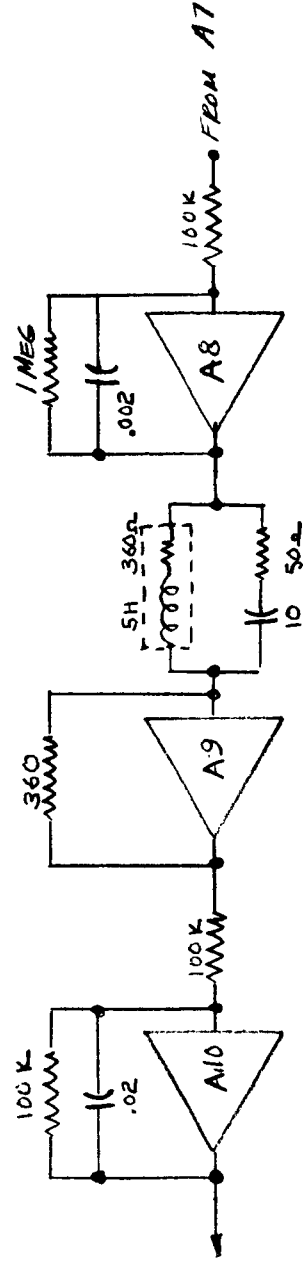


Figure 3.1.9



$$\frac{10\left(1 + 0.009s + \frac{s^2}{140^2}\right)}{(1 + 0.002s)^2 \left(1 + 0.014s + \frac{s^2}{379^2}\right)}$$

Compensation Network
Figure 3.1.10

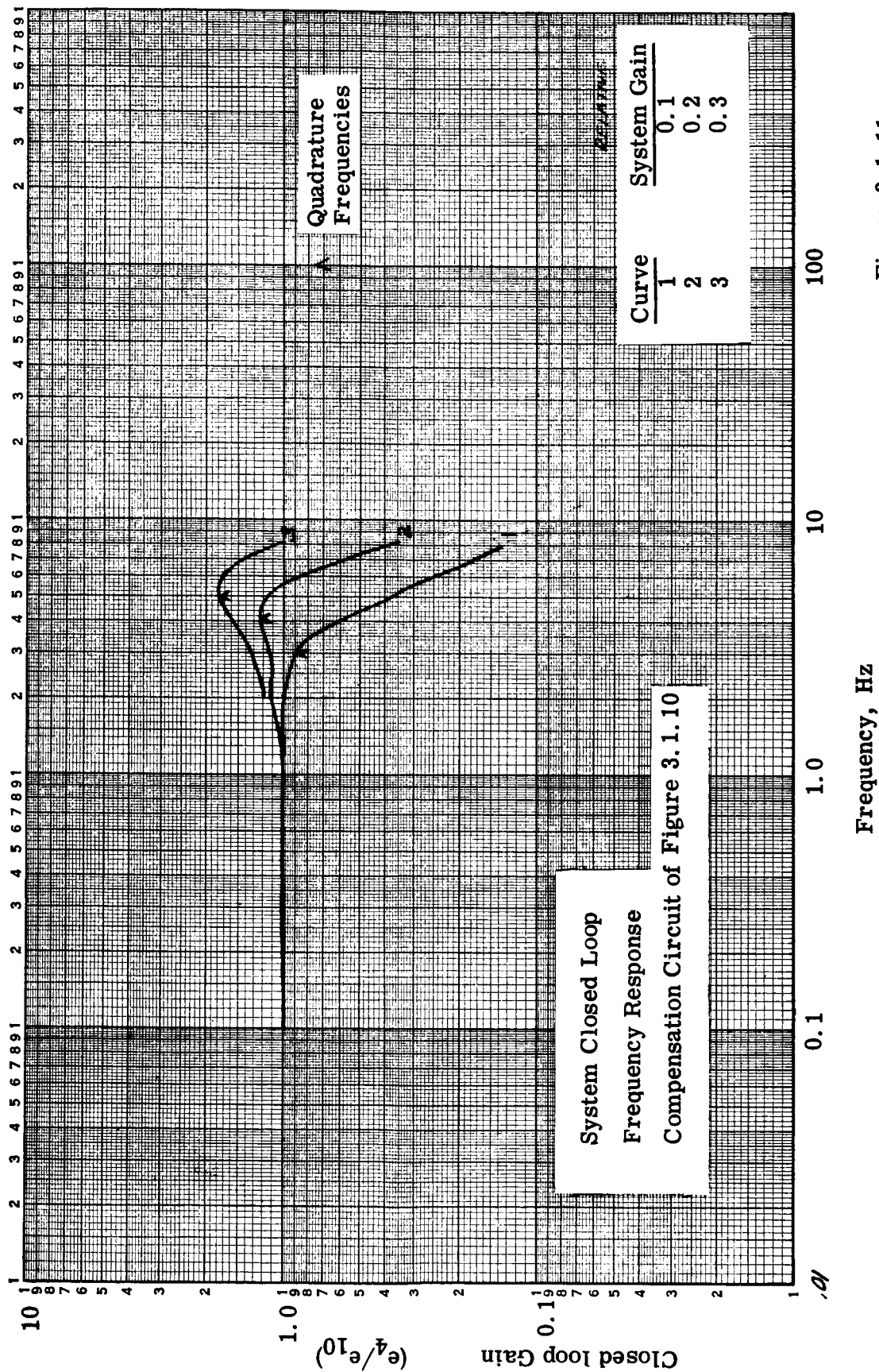


Figure 3.1.11

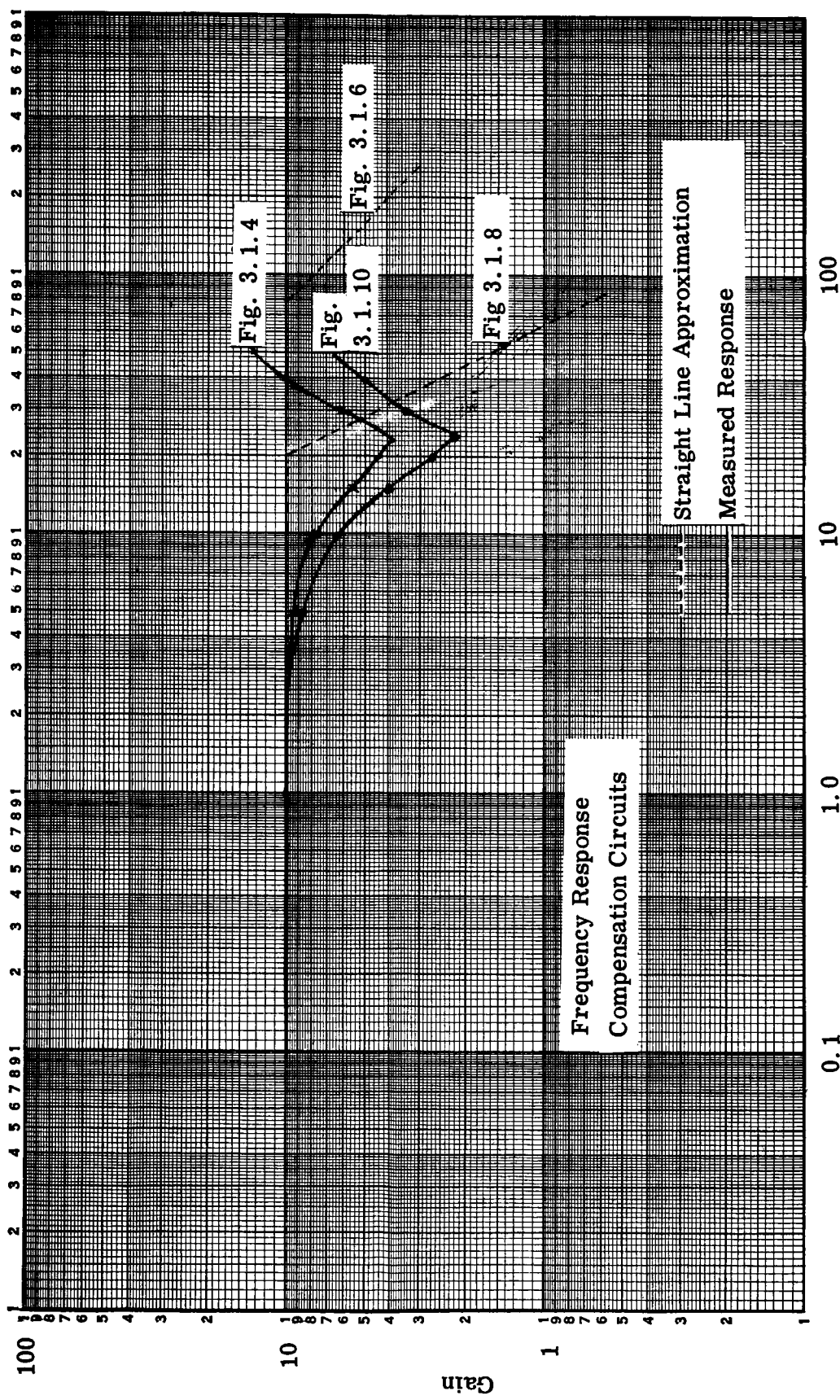


Figure 3.1.12

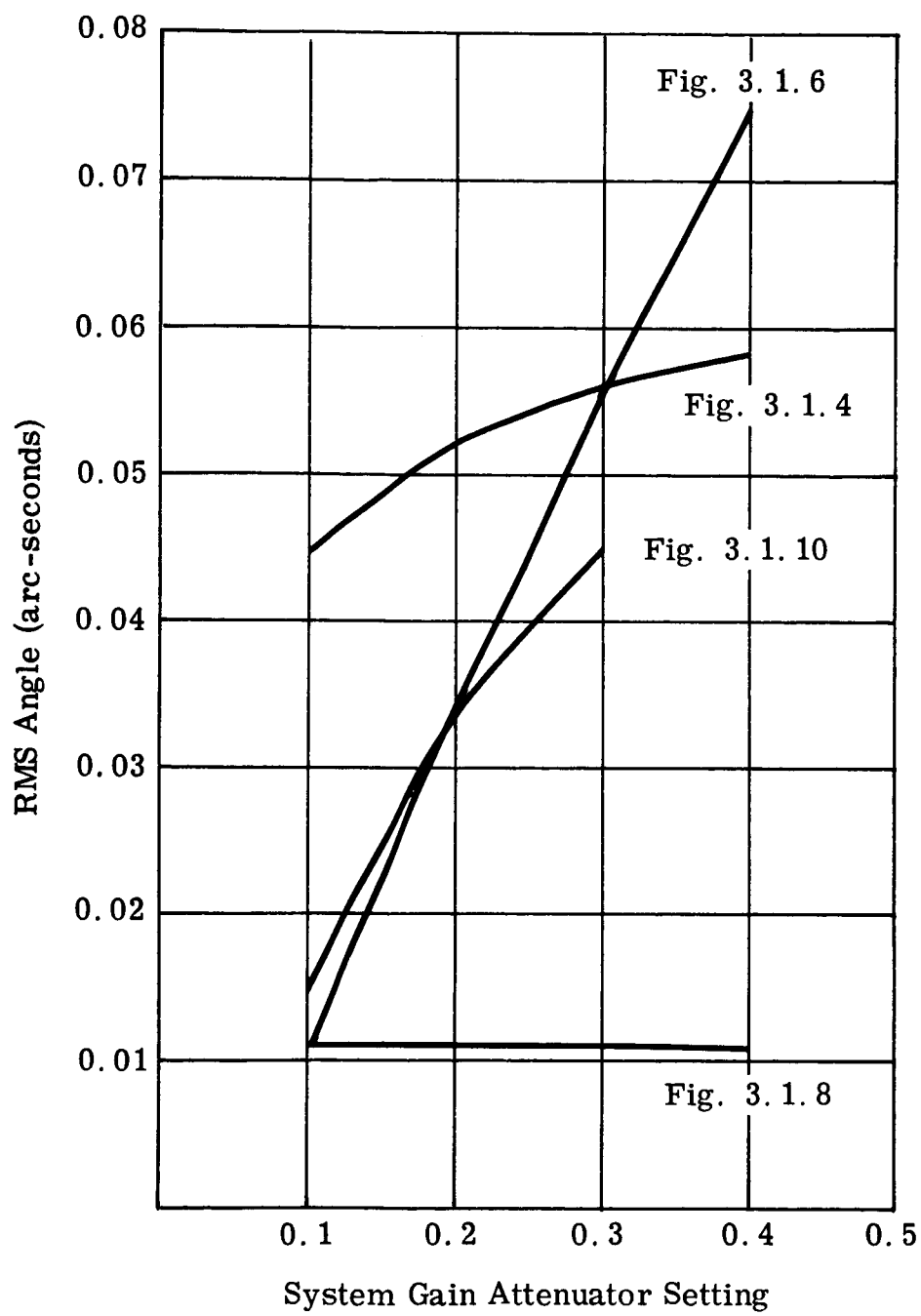


Figure 3.1.13 Control Gyro Error Signal vs. System Gain

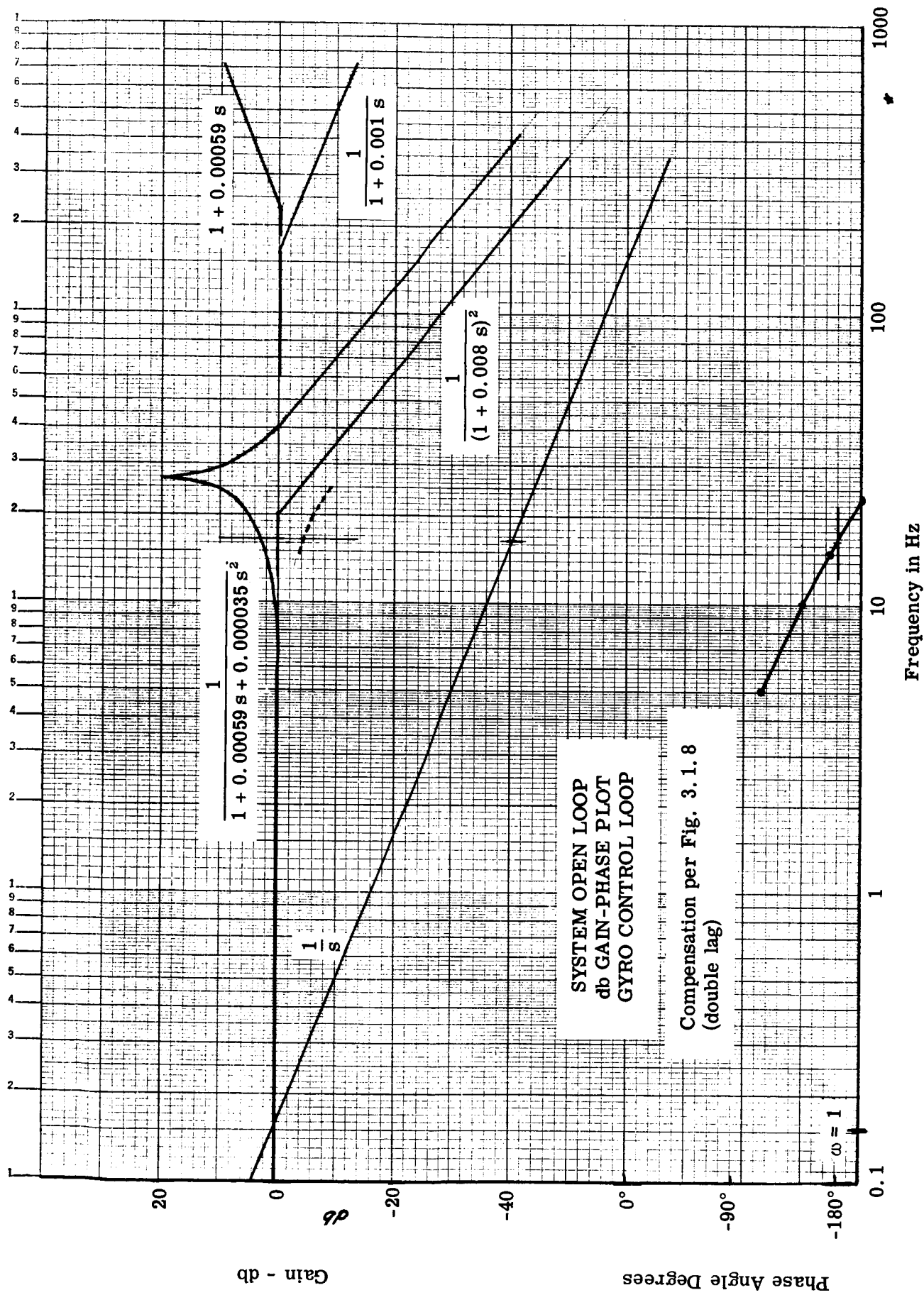


Figure 3.1.14

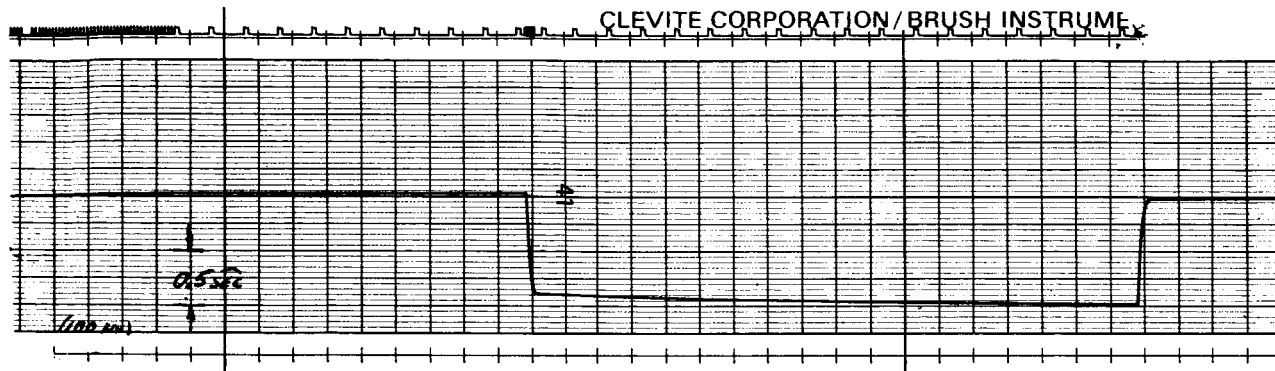
3.2 TRANSIENT RESPONSE TO TORQUE

One significant advantage of a gyro-controlled system compared to a level-only controlled system is its rapid response to transient torque disturbances and fast recovery time. Step input torques were introduced to the system by removing a 26.8 pound lead weight at the actuator end of the structure, and noting the angular deflection of the system as measured by the tilt sensor and GI-V7 gyro. This weight at the end of a 5-foot moment arm generates a 134-ft. -lb. torque. Figure 3.2.1 is a recording of the table tilt resulting from this applied torque with the system disabled, thus providing a measurement of static compliance of the mechanical structure and floor. Figure 3.2.2 (A) illustrates the deflection of the active system with level control; figure 3.2.2 (B) shows the response of the system with gyro control, both tracings are the same scale. Figure 3.2.3 is a 4X magnification of the GI-V7 signal. The conclusions are summarized as follows:

	Peak Transient Deflection (arc-sec.)	Approximate Recovery Time	
		To 0.1 arc-sec.	To 0.01 arc-sec.
System Off (Static Compliance)	0.925	-	-
Level Control	0.6 (EST)	10 sec.	*(10 minutes estimated)
Gyro Control	0.11	0.3 sec.	** <0.3 sec.

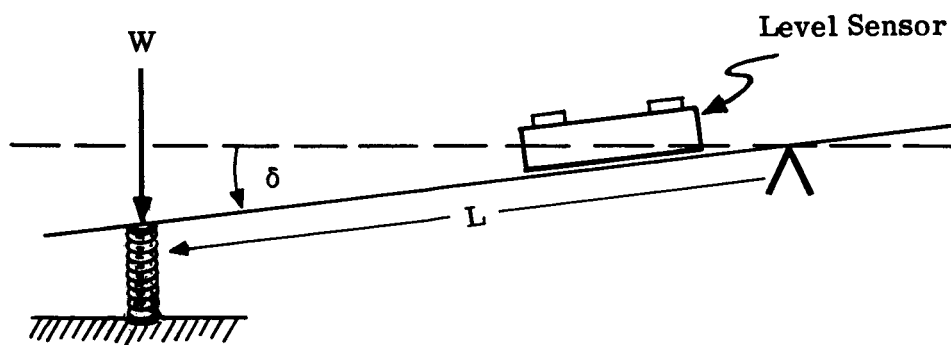
*It appears in figure 3.2.2(A) that a steady-state error of 0.085 arc-sec. results from this applied torque. This is not the case, however, since the tilt error integrator would eventually wipe this error out, resulting in a recovery time of several minutes. Note that the GI-V7 signal returns to zero because it has no DC gain due, in particular, to the applied output axis restraint.

**The GI-V7 output data indicates an offset angular displacement of 0.034 arc-sec. which returns to zero in approximately 28 seconds (see figure 3.2.3); however, the level signal from the level sensor does not indicate this tilt. Since a signal of this magnitude and time duration would be easily detectable by the level sensor even with its associated 10-second data filter, it must be concluded that the GI-V7 signal represents float decentering or some other phenomenon, and does not represent platform tilt. The 28-second recovery transient shown in figure 3.2.3 is actually that of the GI-V7 monitor gyro from this disturbance.



Compliance of Platform Jacking Mechanism and Supporting Structure

$$W = 26.8 \text{ lb.}$$



$$W = 26.8 \text{ lb.}$$

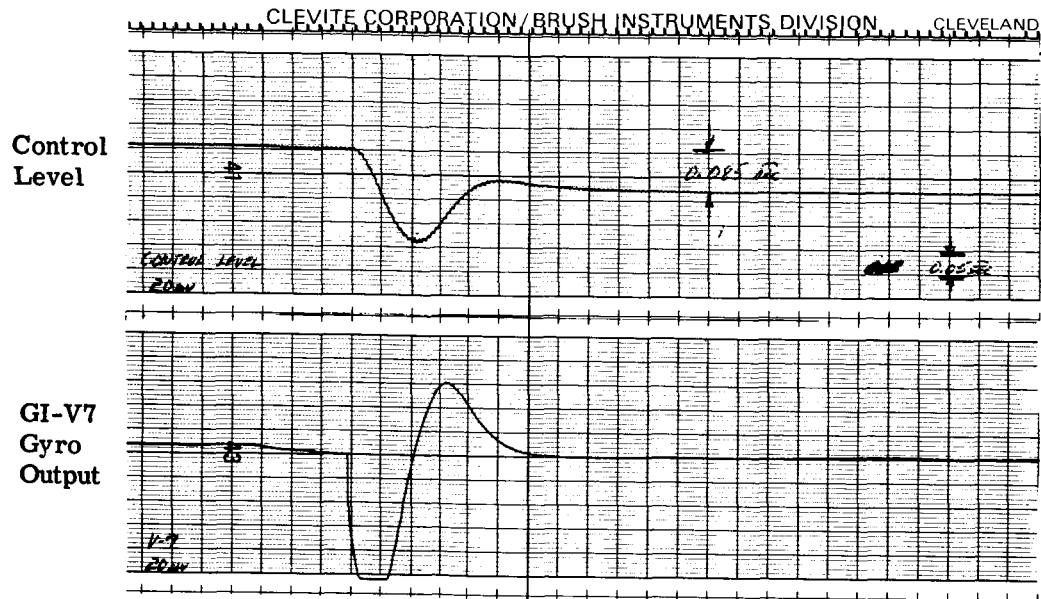
$$L = 5 \text{ ft.}$$

$$\delta = 0.93 \text{ arc-sec.}$$

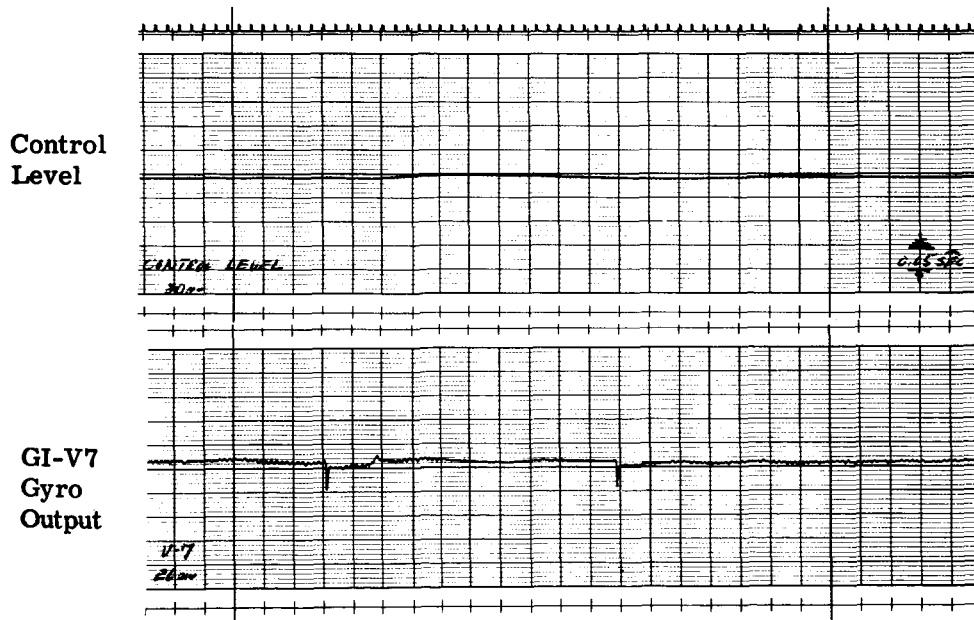
$$\text{Compliance} = 6.95 \times 10^{-3} \text{ arc-sec/ft. -lb.}$$

Figure 3.2.1

Transient Response to 134 ft. -lb. Torque Disturbance



(A) Level Control Mode



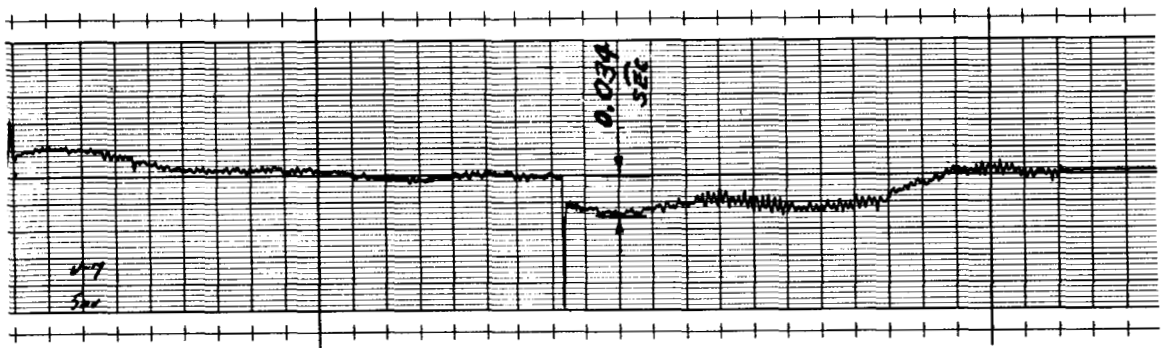
(B) Gyro Control Mode

Figure 3. 2. 2

Transient Response to 134 ft. -lb.

Torque Disturbance to Test Table

Gyro Control Mode



GI-V7 Gyro Output
(Expanded Scale)

Figure 3. 2. 3

3.3 LEVEL LOOP OPERATION

The next loop to be considered was the accelerometer-to-gyro loop, sometimes called level or erection loop. This loop, which couples the system to linear acceleration, and hence local vertical, is essential for providing long-term stability in the presence of gyro drift.

Both transient and frequency response measurements were made at various level gain settings. Step input acceleration was obtained by introducing actual table tilt; periodic acceleration inputs were simulated by electrical signals. Figure 3.3.1 illustrates the transient response of the system to linear acceleration for three settings of the level attenuator gain control. An attenuation setting of 0.6 in the loop provides a response which appears critically damped and whose time constant is approximately 7.5 seconds.

Figure 3.3.2 shows the relative angular frequency response of the platform to linear acceleration. Acceleration was simulated electrically while table angular response was determined by the GI-V7 gyro. The characteristics of this loop are primarily determined by the Tiltmeter Filter, since straight gain in this loop, for example, with a gain setting of 0.6, would provide a first-order response with a characteristic time of 0.42 seconds.

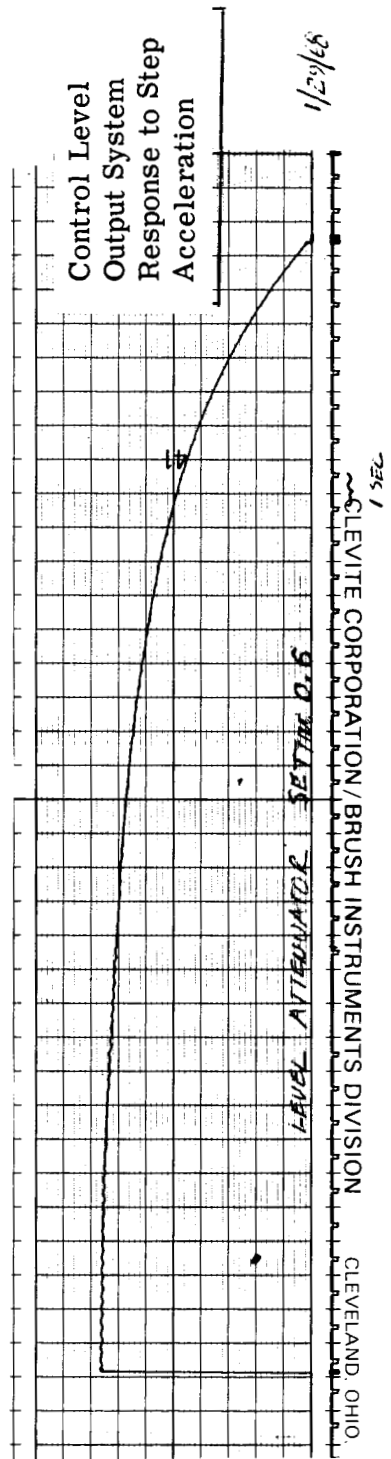
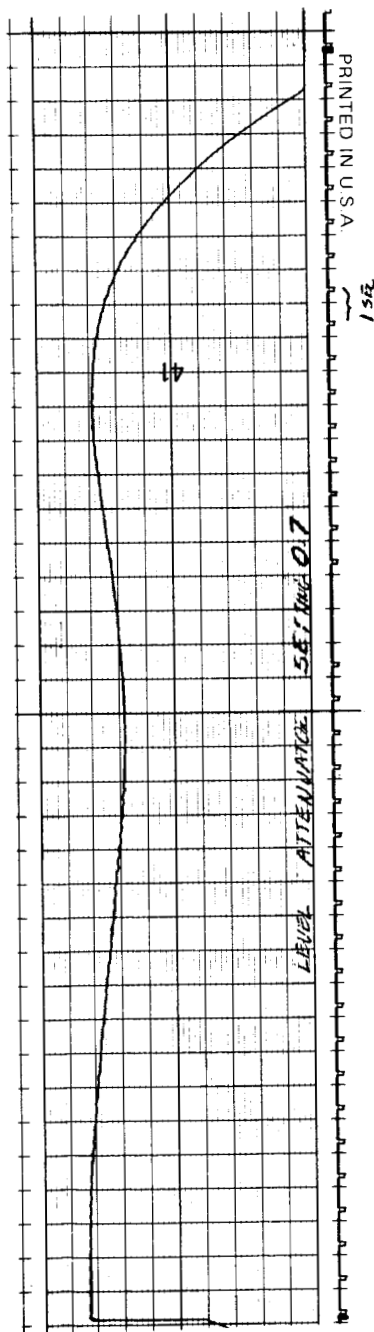
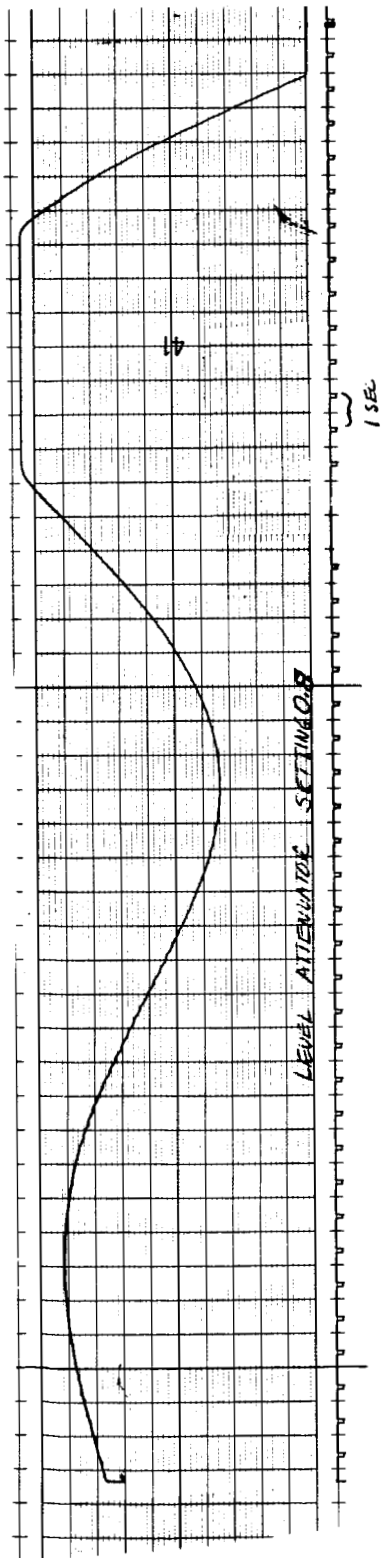


Figure 3.3.1

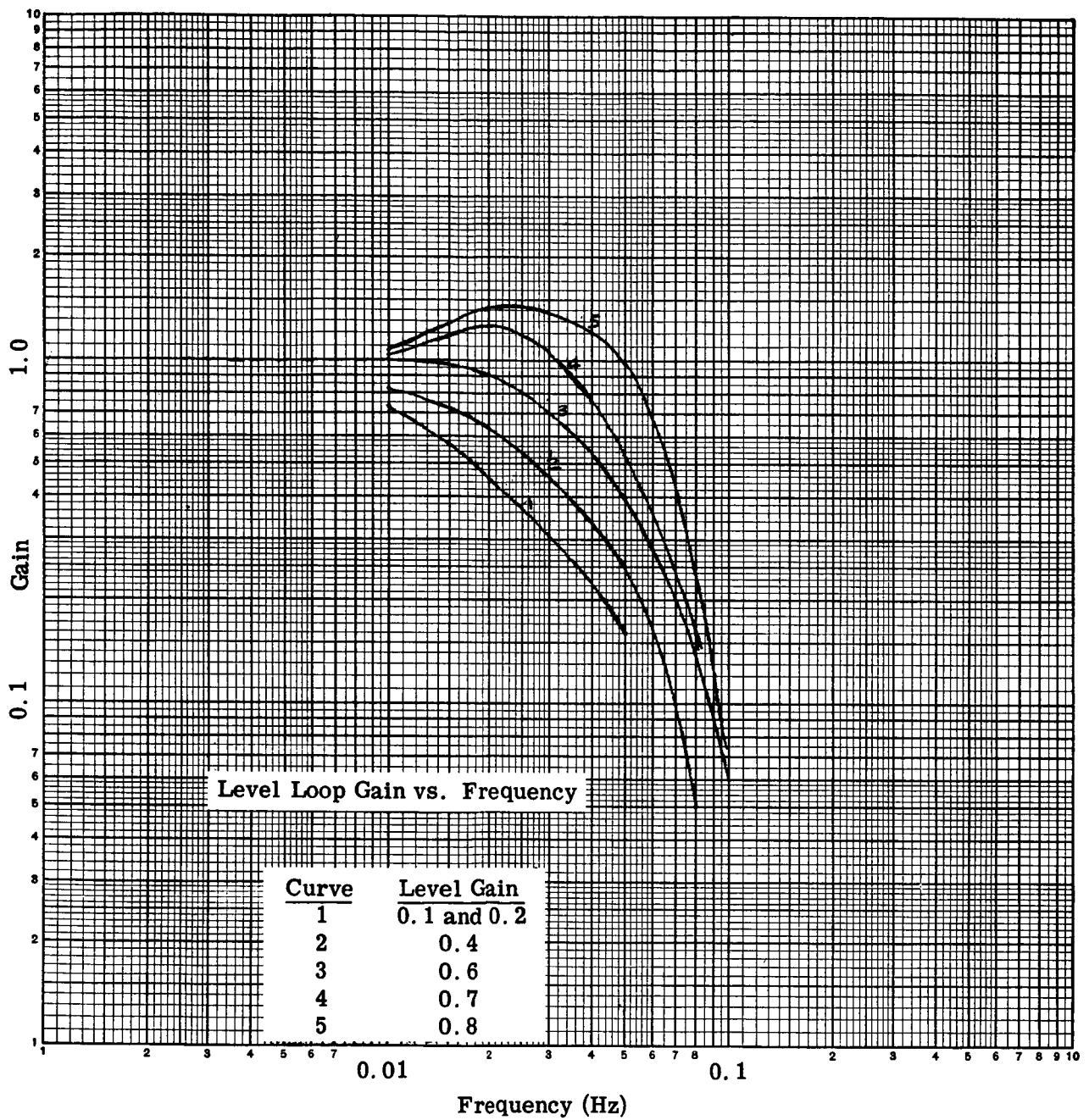


Figure 3.3.2

3.4 LONG-TERM LEVEL STABILITY

The long-term level stability of the system ($\omega \leq 0.01$ rad./sec.) was monitored by the tilt sensors, both the controlling sensor and either one or two monitor levels (higher frequency data, measured by the GI-V7 monitor gyro, seismic and gyro noise measurements are discussed in section 3.5). Of particular importance is the distinction between the absolute or "true" level error and level control loop error signal as measured by the output signal of the controlling level sensor. A greater significance is placed on this latter signal because it represents a direct measurement of system capability without regard to the accuracy of the actual sensor used.

To illustrate more fully the time variance of level error data, a summary of the data for the entire 78-day test period is first presented (figure 3.4.1) then is shown a 12-day test run with data points plotted every six hours (figure 3.4.2), followed by a test run with data recorded at one-hour intervals (figure 3.4.3), and finally a sample of a continuous data recording is presented in figure 3.4.4.

The level error data shown in figure 3.4.1 is normalized; that is, the level signal at the start of each run is taken as zero and the subsequent data points represent deviations from the initial reading. Relative error values between each run are not shown because many variables (such as recorder re-zeroing, mechanical and electrical adjustments, and interchange of instruments and sensors) were introduced between each run; there is no reason to believe that for a continuous test run the level error signal would not be bounded within the limits shown in figure 3.4.1 for an indefinite period.

Runs No. 19A and 20, made in the level control mode, were not plotted due to the fact that in most instances the data was greater than the maximum value of the scale chosen for the data presentation.

Of particular interest in figure 3.4.1 is the high excursion of run 1, a somewhat lower ramp observed in run 2, and then another large excursion appearing again in run 12. Both excursions represent a disturbance occurring immediately after initial start-up of the electronics. The system electronics was shut down only once in the course of these tests, and that was just prior to run 12. The fact that the time constant appears to be approximately three to five days is not completely understood. An examination of the loop diagram

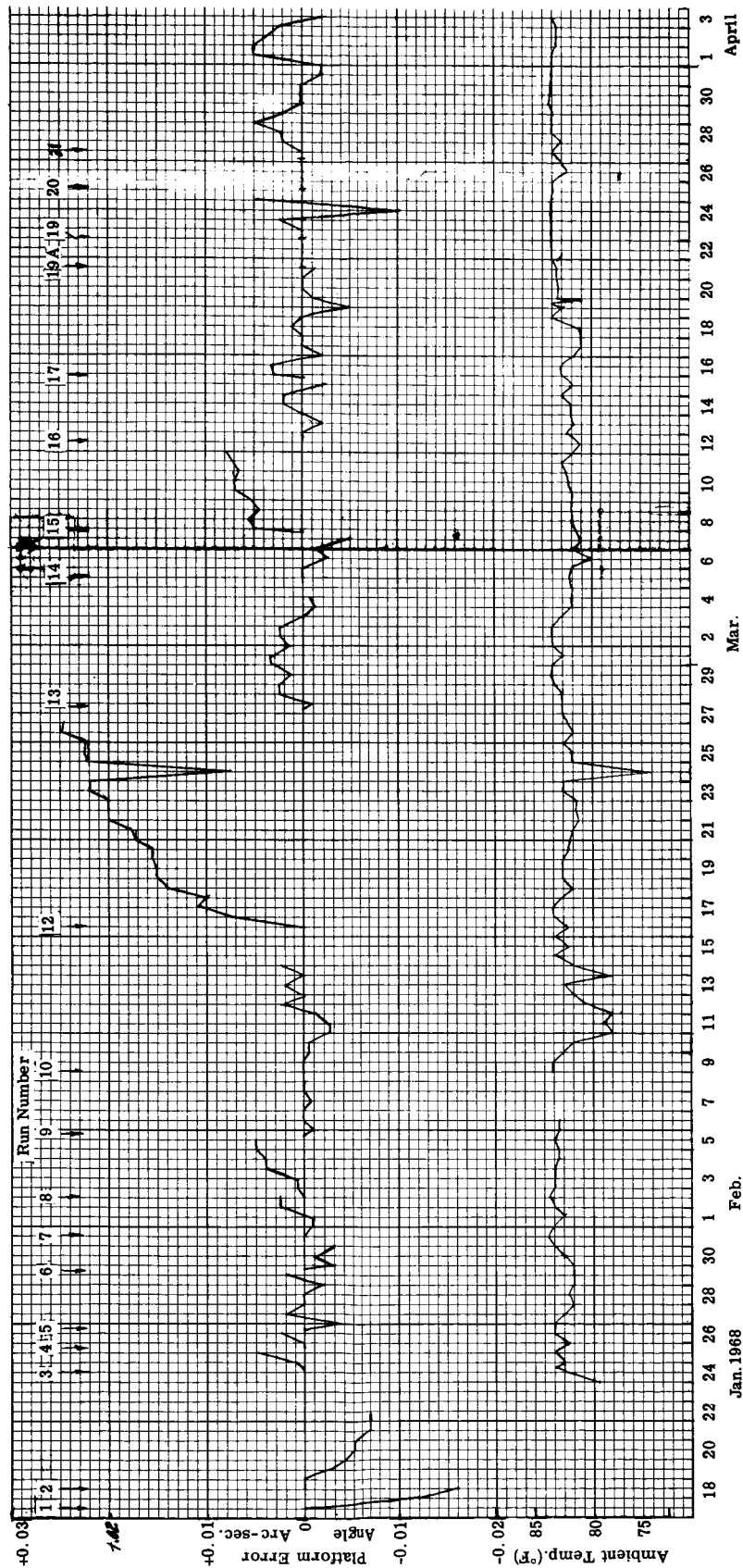


Figure 3.4.1

reveals that in all probability, the error observed results from an integrator drift, since an offset in all other electronic components would not manifest itself in a long-term offset of the control accelerometer error signal. In contrast, the GI-T2 gyro was replaced just prior to Run 17, without de-energizing the electronics, and the system was put into operation with no unusual disturbances observed. Room ambient temperature is also presented in figure 3.4.1. A definite correlation between temperature and level error signal is observed. This is particularly noticeable in run 12.

Although the high-frequency noise, as measured by the GI-V7, varied considerably between different system configurations and gain settings, the long-term stability was not noticeably effected. Table I shows the conditions for each run.

A more complete record of the data collected during run 12 is presented in figure 3.4.2. In addition to the level error signal, the following data is presented:

1. Platform monitor level output
2. Floor angle monitor output (two units)
3. Servo shaft angle data calibrated in table tilt angle


An unsuccessful attempt was made to relate table tilt, floor tilt, and servo shaft angle, but no obvious correlation exists. Temperature variations and unequal expansions alone may be a significant error when making measurements in the fractional arc-second region. The polarities shown in figure 3.4.2 are arranged such that

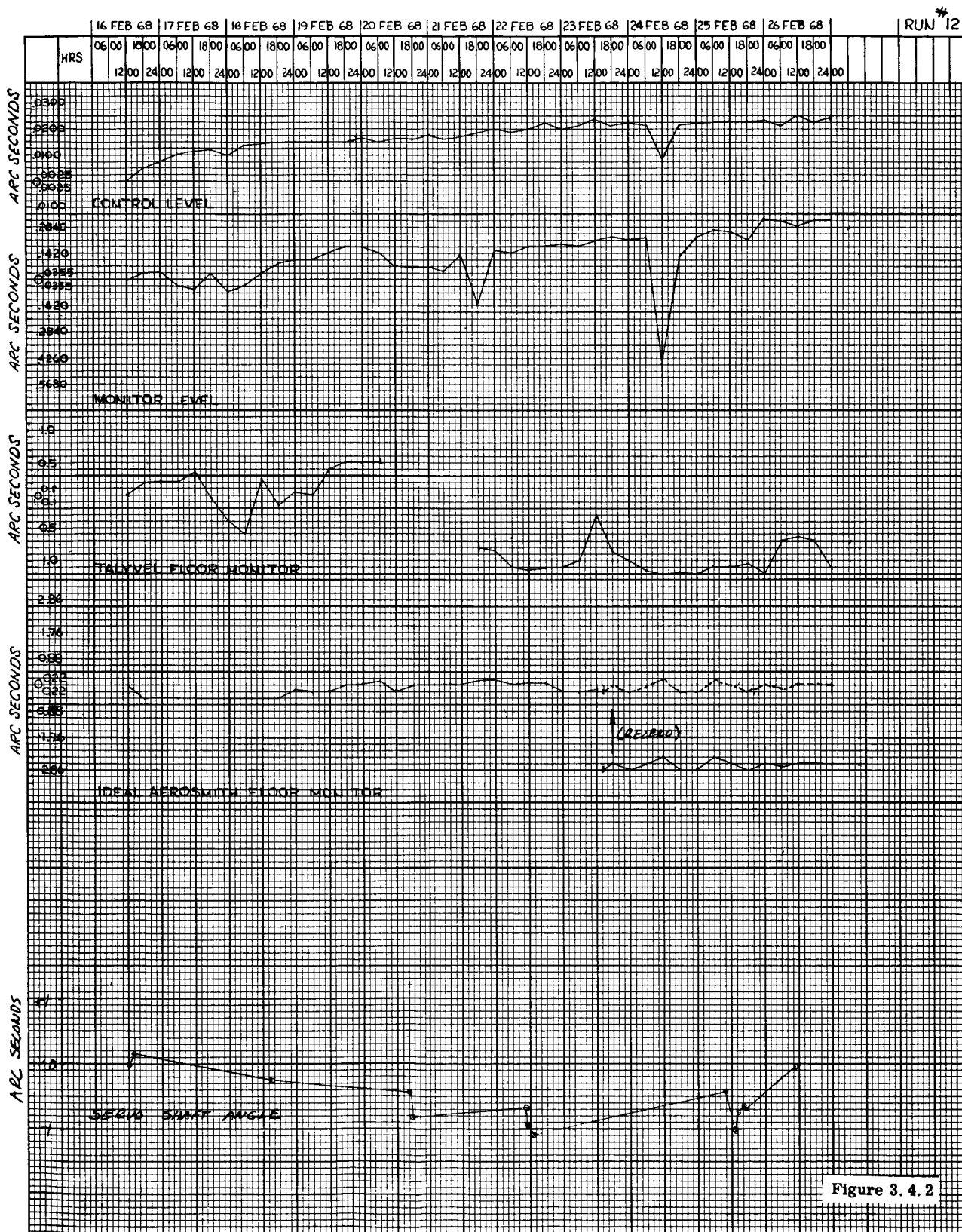
$$\text{Monitor Level} = \text{Servo Angle} + \text{Floor Tilt}$$

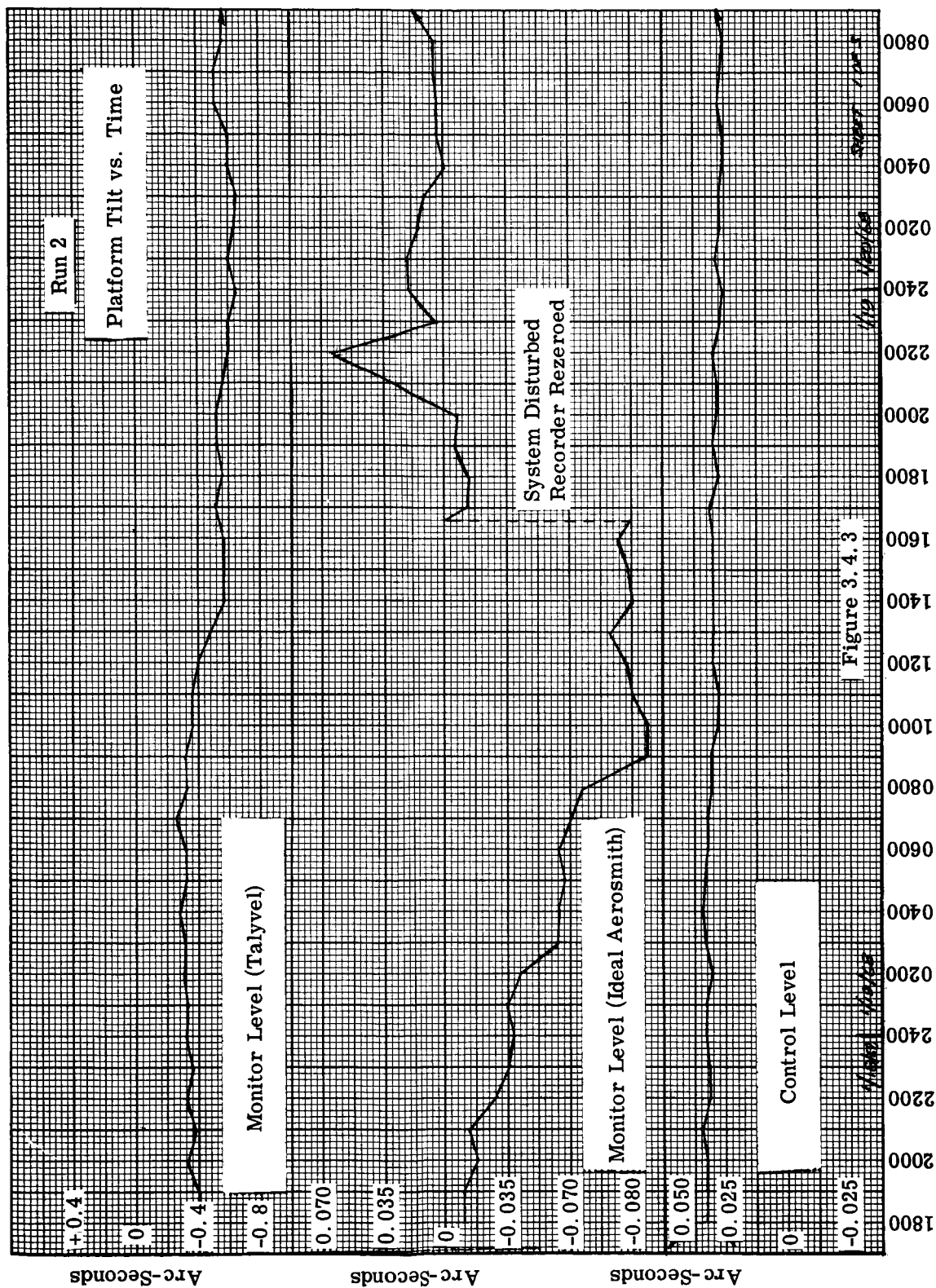
The servo shaft angle data was taken at sporadic intervals, and the data points which indicate servo angle are shown connected by straight lines in figure 3.4.2.

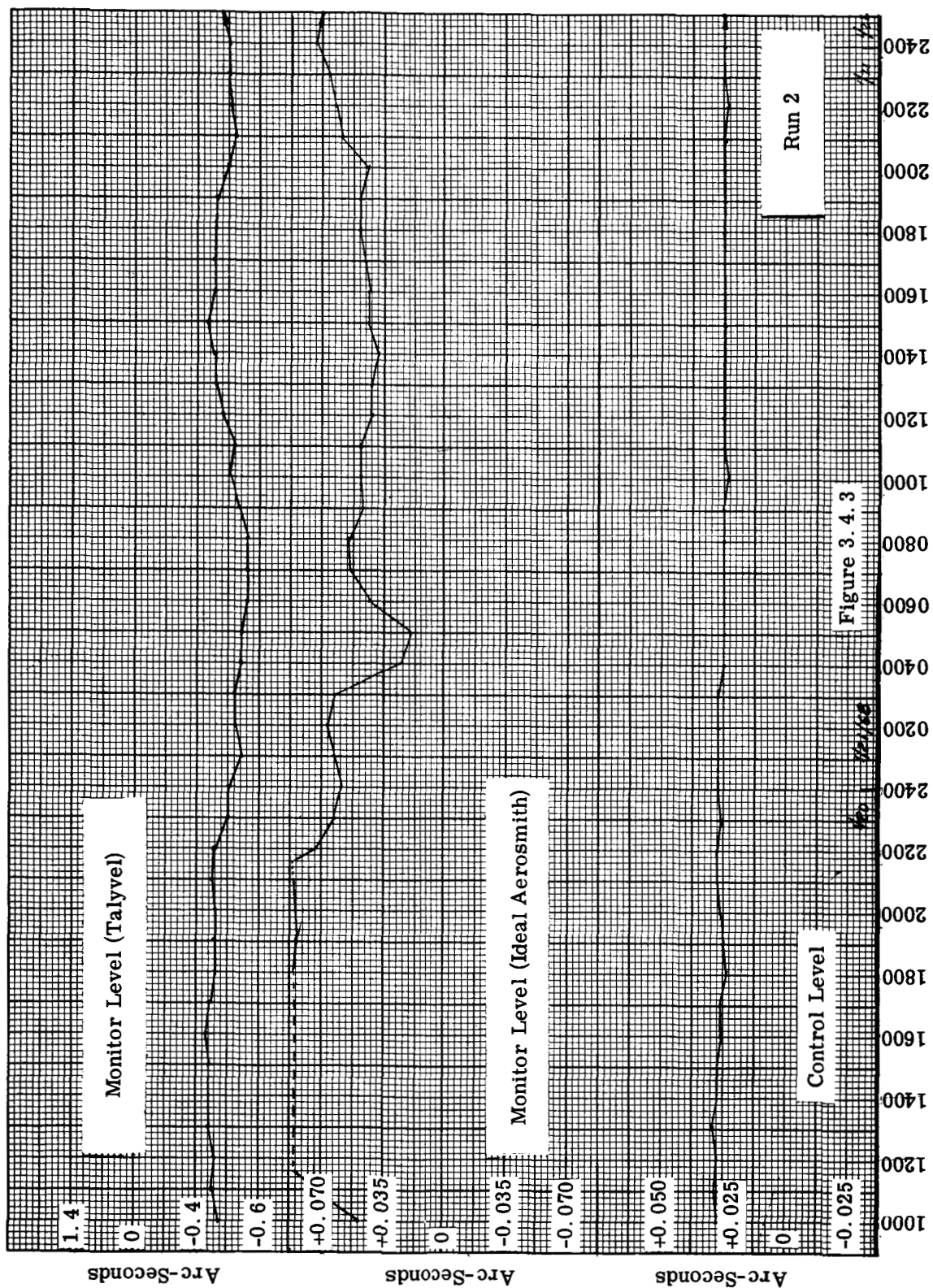
Figure 3.4.3 indicates a considerable lack of agreement between the two monitor levels. The Ideal Aerosmith Monitor Level data indicates the relative error between the control level and the monitor level (the two identical units placed side by side on the special plate described in the first section). A peak differential angle of approximately 0.1 arc-second is observed. It is quite apparent that a determination of level sensor accuracies

TABLE I
LEVEL ERROR RUN CONDITIONS

Run No.	SG Gain	System Gain	Level Gain	Servo Compensation
1	0.5	0.1	0.5	Fig. 3.1.6
2	0.5	0.3	0.5	Fig. 3.1.8
3	0.5	0.1	0.5	Fig. 3.1.10
4	0.5	0.2	0.6	Fig. 3.1.6
5	0.5	0.1	0.6	Fig. 3.1.6
6	0.5	0.1	0.7	Fig. 3.1.8
7	0.04	0.1	0.7	
8	0.04	0.1	0.7	
9	0.04	0.1	0.7	
10	0.04	0.15	0.7	
11	(Aborted)			
12	0.04	0.15	0.7/0.3	
13	0.02	0.1	0.2	
14	0.02	0.1	0.06	
15	0.02	0.1	0.7	
16	0.02	0.1	0.7	
17	0.02	0.1	0.7	
18	0.02	0.1	0.7	
19	0.02	0.1	0.7	
20	0.02	0.1	0.7	







and the evaluation of a control system with regard to its "absolute" level error would involve the simultaneous recording of many sensors, whereupon it becomes possible to separate instrument variations statistically from "true" level error to a great extent.

The data in figure 3.4.4 illustrates the typical short-term level data recorded throughout the test period. It should be noted, however, that the level signals are filtered by a 10-second filter to prevent high-frequency translational motions and sloshing of the mercury pools in the Ideal-Aerosmith Level from obscuring the tilt data. Higher frequency angular excursions, greater than 0.10 rad./sec., which are evident in the GI-V7 monitor gyro data, are discussed in section 3.5. The time scale for figure 3.4.4 is 1.5 millimeters per minute.

Figure 3.4.5 makes a direct comparison between gyro and level (only) control. Peak-to-peak variations of the control level signal are approximately 0.01 arc-second in the gyro control, whereas in level control, the error becomes an order of magnitude greater.

Figure 3.4.6 is included to illustrate the response of the system to a step change in control gyro drift. The gyro command signal, which is a proportional plus integral of the platform tilt signal, provides gyro drift compensation. The initial tilt response of the system occurs within seconds, resulting in gyro drift compensation by the accelerometer output signal through straight gain. The integrator portion of the network, which provides very high d-c gain, eventually takes up the required gyro compensation and allows the tilt signal to return to zero. Step changes of gyro drift are considered abnormal and resulting from a failure condition; however, this data demonstrates the self-correcting feature of the system and the fact that no steady-state tilt error results from constant gyro drift. Small bounded errors would exist, of course, in the presence of gyro drift ramp. High-quality integrators, stable to better than 10 PPM, could be used in this manner to provide automatic earth rate correction in a two-axis system, thus allowing the system, on a steady-state basis, to be independent of azimuth position.

Figure 3.4.7 represents one of four earthquakes which were sensed by the system during the course of this experiment. This particular earthquake occurred near the Kurile Islands on January 29, 1968, and according to press reports, the tremor was measured at 7.2 on the Richter scale at Berkeley, California. While the data is not sufficient to separate tilt from

linear acceleration on the level signals, the monitor gyro indicates a peak-to-peak platform tilt of approximately 0.1 arc-second. One conclusion that can be drawn from this experience is that the system would be less susceptible to linear accelerations at the characteristic frequency observed (0.05 Hz) if the upper frequency cutoff of the erection loop were reduced. Note in figure 3.3.2 that the table response to linear acceleration is down only 8 db at 0.05 Hz at a level gain setting of 0.6. An examination of the seismic data (figure 3.5.1) reveals a predominant 0.05 Hz component. This would seem to indicate that this frequency is one of particular interest in the design of an effective tilt and angular vibration isolation system. The degree to which the system can be decoupled from the level loop must be weighed carefully against the gyro drift requirements, since a reduction in bandwidth of the level loop requires extended gyro control in the low frequency region, an area of poor gyro performance.

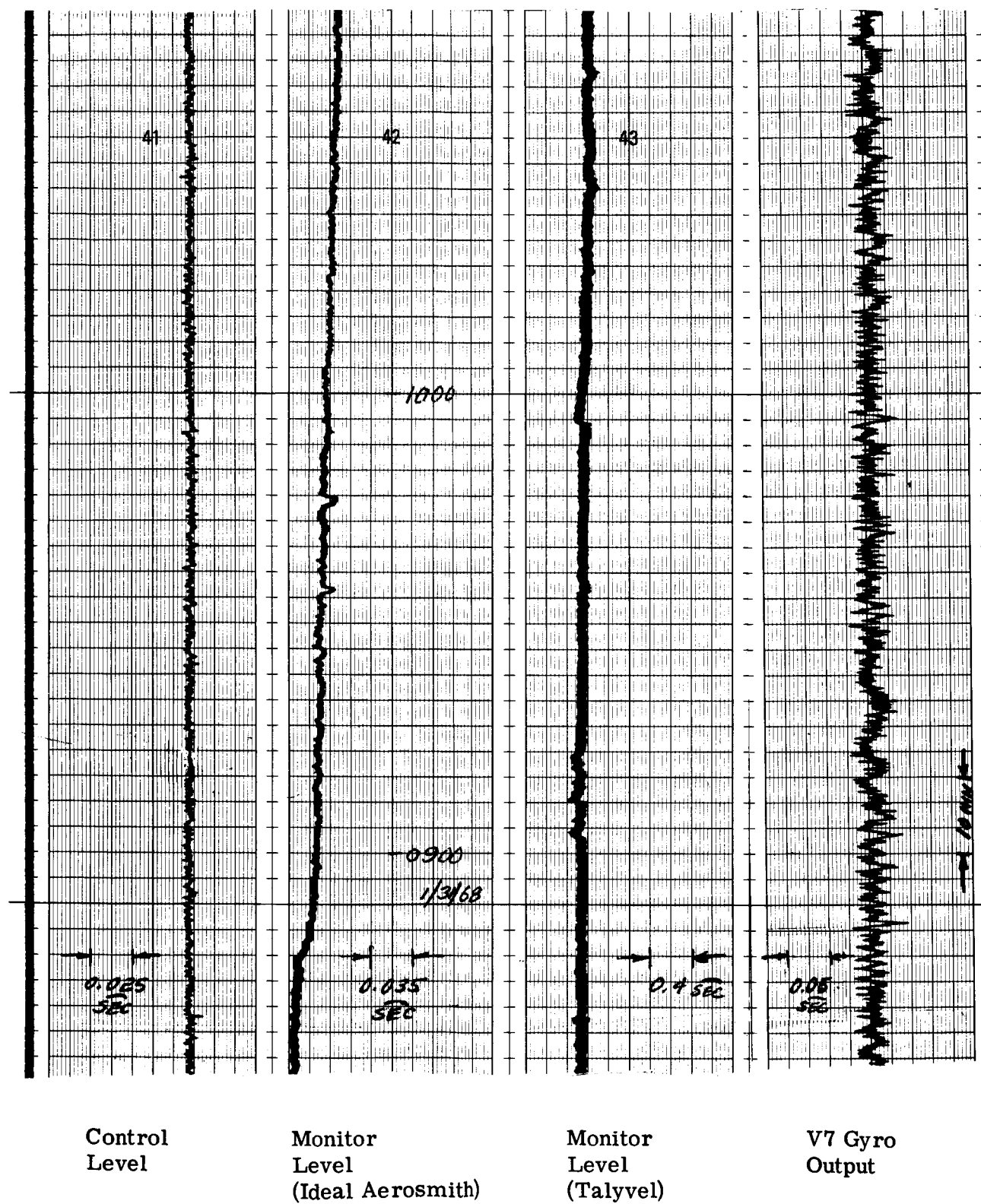
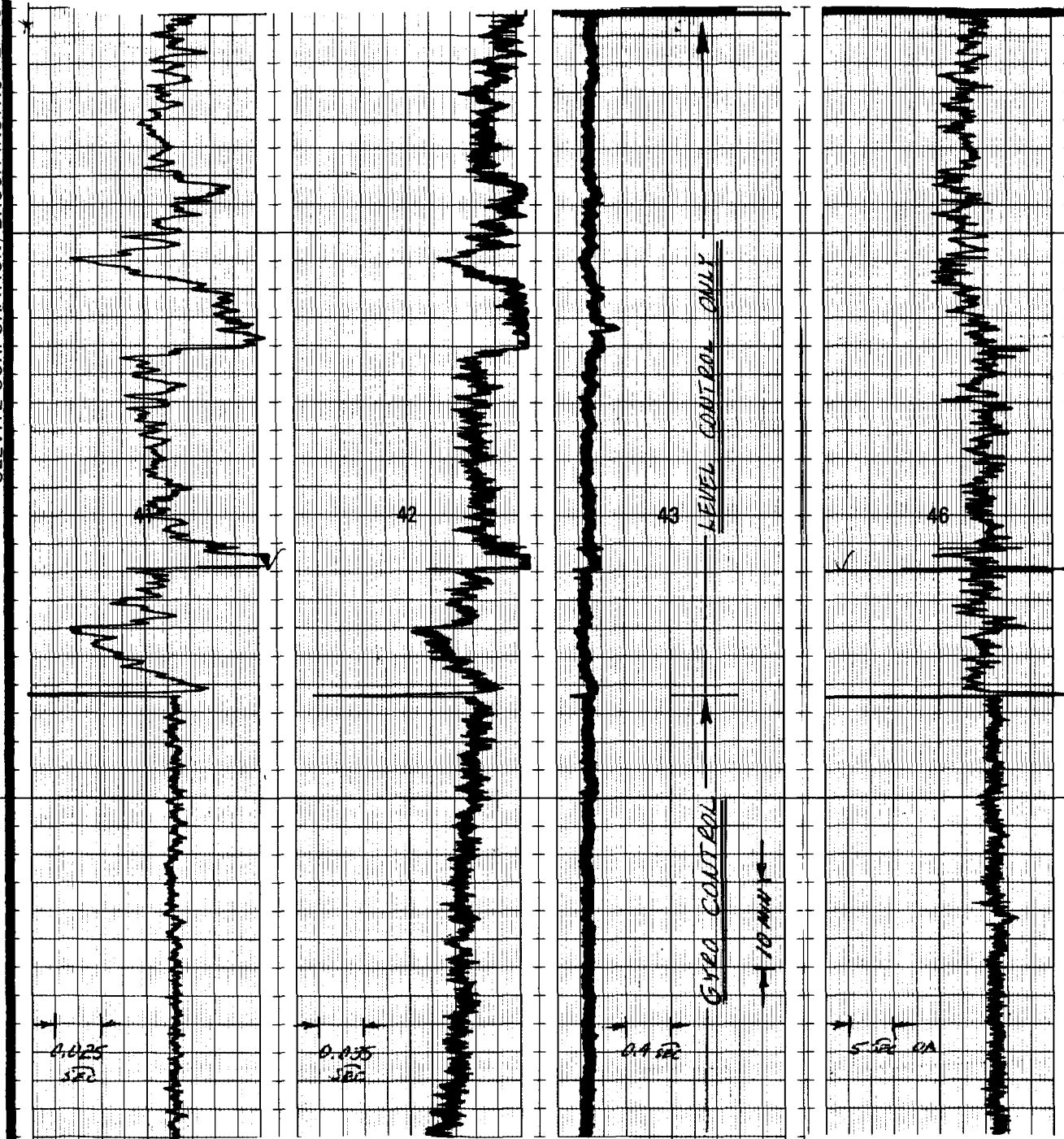


Figure 3. 4. 4



Control Level

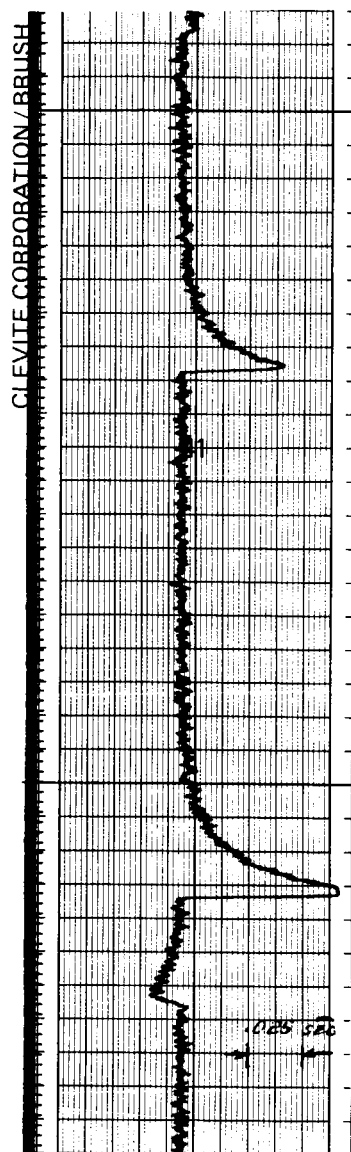
Monitor Level
(Ideal Aerosmith)

Monitor Level
(Talyvel)

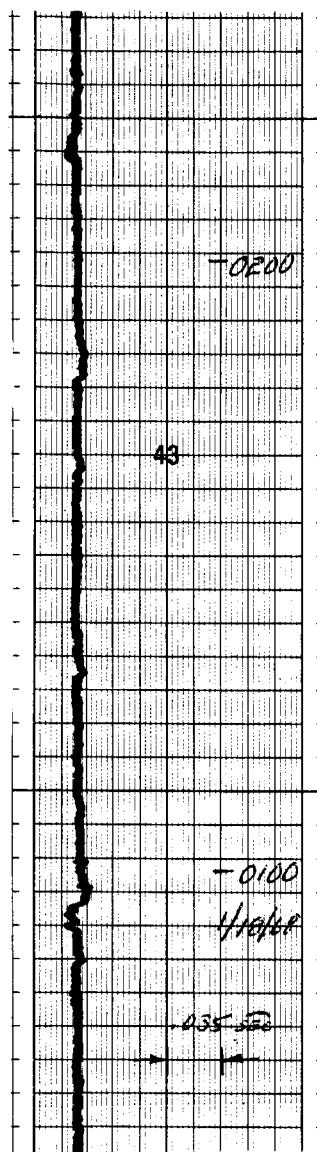
V7 Gyro
Output

1/25/68

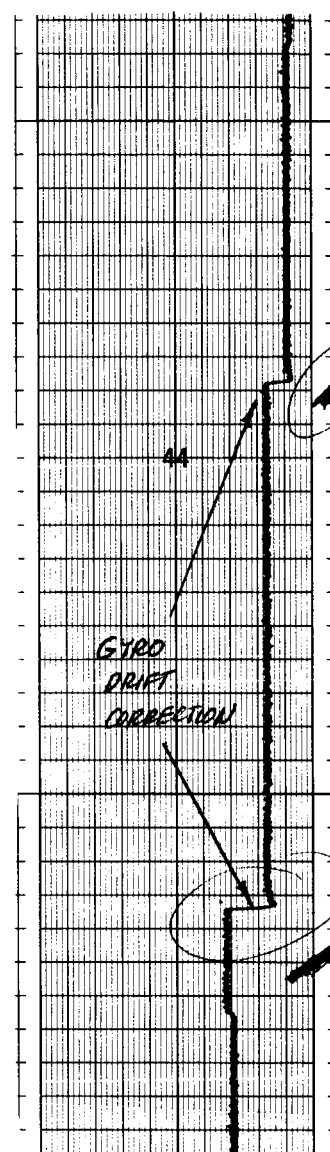
Figure 3.4.5



Control Level



Monitor Level
(Talyvel)



Gyro Command
(Compensation)

Figure 3. 4. 6

Part of Run 1

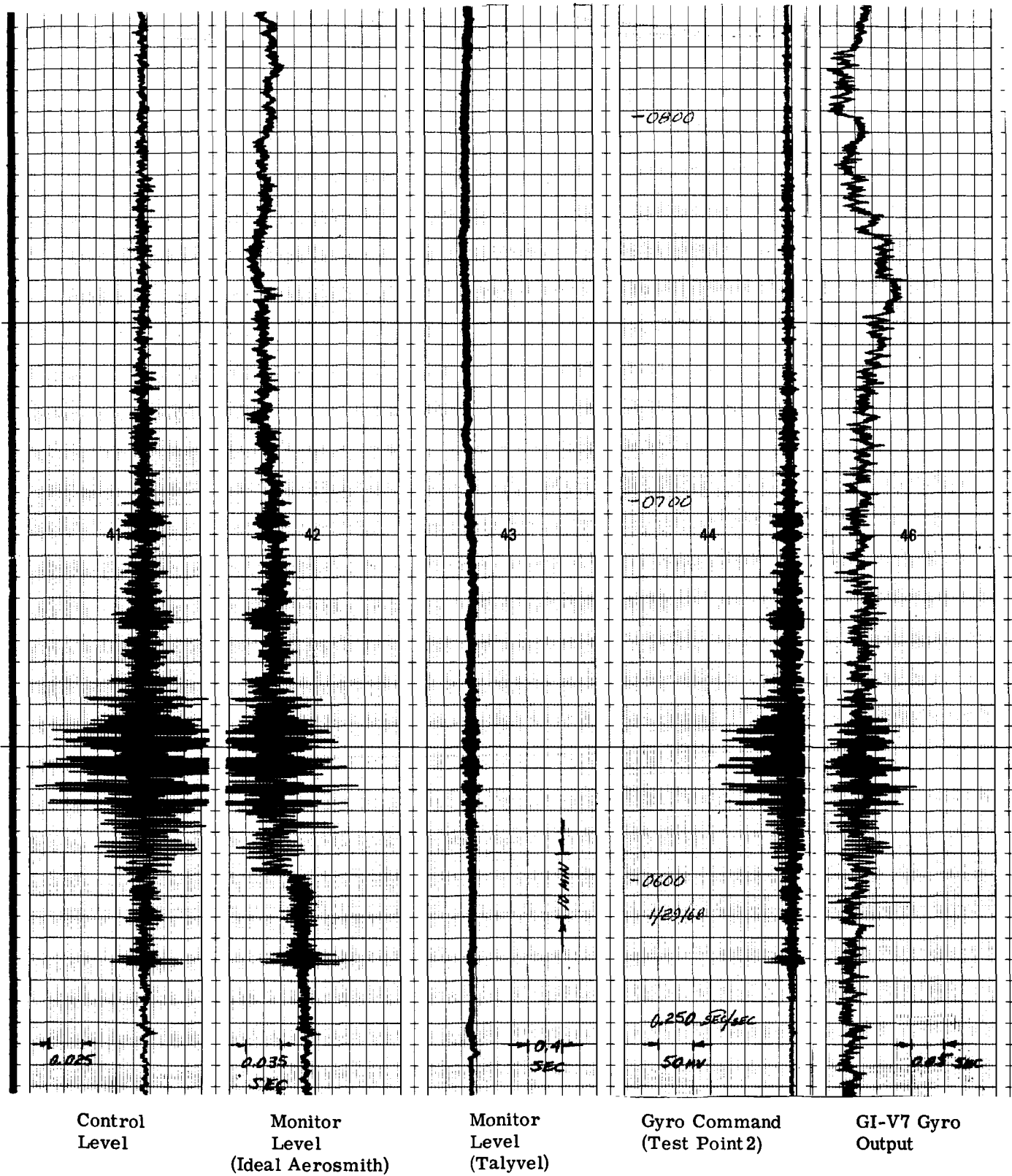


Figure 3.4.7

3.5 SHORT-TERM LEVEL STABILITY AND GYRO NOISE

Since the main object of this program is to study the possible improvement in performance of a leveling loop by adding a gyroscope, it is natural to use a second gyro for evaluation purposes. In particular, since a gyroscope represents an almost ideal angle transducer (it is relatively insensitive to linear motion), and since its bandwidth extends into the frequencies of interest, it will be useful not only for instrumenting platform performance, but also for measuring angular ground inputs to the system.

Figure 3.5.1 represents a tracing of ground motion as measured by the GI-V7. To ascertain that the excursions indicated represent seismic motion and not some other phenomenon, two experiments were tried: 1) the V7 output was observed under the same conditions, but with wheel on and wheel off, and 2) simultaneous GI-V7 and GI-T2 data were taken for comparison. Figure 3.5.2 illustrates the effect of seismic noise input sensed by the gyro when the wheel is rotating, and in comparison, random gyro float motions existing with the wheel idle. Figure 3.5.3 shows almost identical outputs from the two gyros which must, therefore, represent a response to true input information.

The next step was to observe the short-term stability of the platform as the control gyro gain was increased from zero to the maximum stable setting. The GI-V7 and level sensor signals are shown in figure 3.5.4; i. e., for level gain settings of 0, 0.1, 0.2, 0.3, and 0.4.

As expected, a reduction of seismic noise was observed on both the level sensor and GI-V7 output traces as the gyro gain was increased. However, an increase in high frequency noise with gain increase is evident in the gyro output, but not in the (filtered) level signal. The amplitude of this signal, in the worst case, is about 0.08 arc-second peak, and the peak seismic excursion is in the order of 0.02 arc-second. Clearly, a noise of this magnitude, generated within the system, is intolerable.

The predominant noise frequency observed occurs at about 2-1/4 Hz and was traced to a wheel-hunt condition in the GI-T2. This phenomenon, which is an oscillatory variation between gyro wheel position with respect to that of its rotating magnetic field, can be caused by non-uniformity of magnetic field rotational speed, irregular torques in the spin bearing, or

physical rotary motion of the motor stator, any of which will disturb the motor-wheel system causing it to ring at its equivalent spring-mass natural frequency. The observed increase in system wheel hunt noise with increased servo gain suggests that there be further investigation of the possibility of a control servo instability created by the coupling of the control system into the spin motor-wheel system, either through direct gyro misalignment or through higher order phenomena existing in the mechanics of the entire structure. The predominant manner by which the oscillatory torque about the gyro spin axis is coupled to the output axis, and hence the platform, is believed to be via a radial displacement sensitivity of the gyro pickoff. The GI-T2, being a paddle-damped gyro, has relatively low damping about the spin axis, and this could also have been a contributory factor.

The following data illustrates that both wheel supply frequency instability and mechanical disturbances have been contributors to the wheel hunt condition. The clock frequency for the GI-T2 wheel supply was originally generated by doubling the 400 Hz GI-V7 wheel supply, which, in turn, was clocked by a built-in bridge-type oscillator. Short-term frequency variations (probably better described as phase variations) too small to be easily measured, can be of sufficient magnitude to spike gyro wheel hunting as shown by figure 3.5.5.

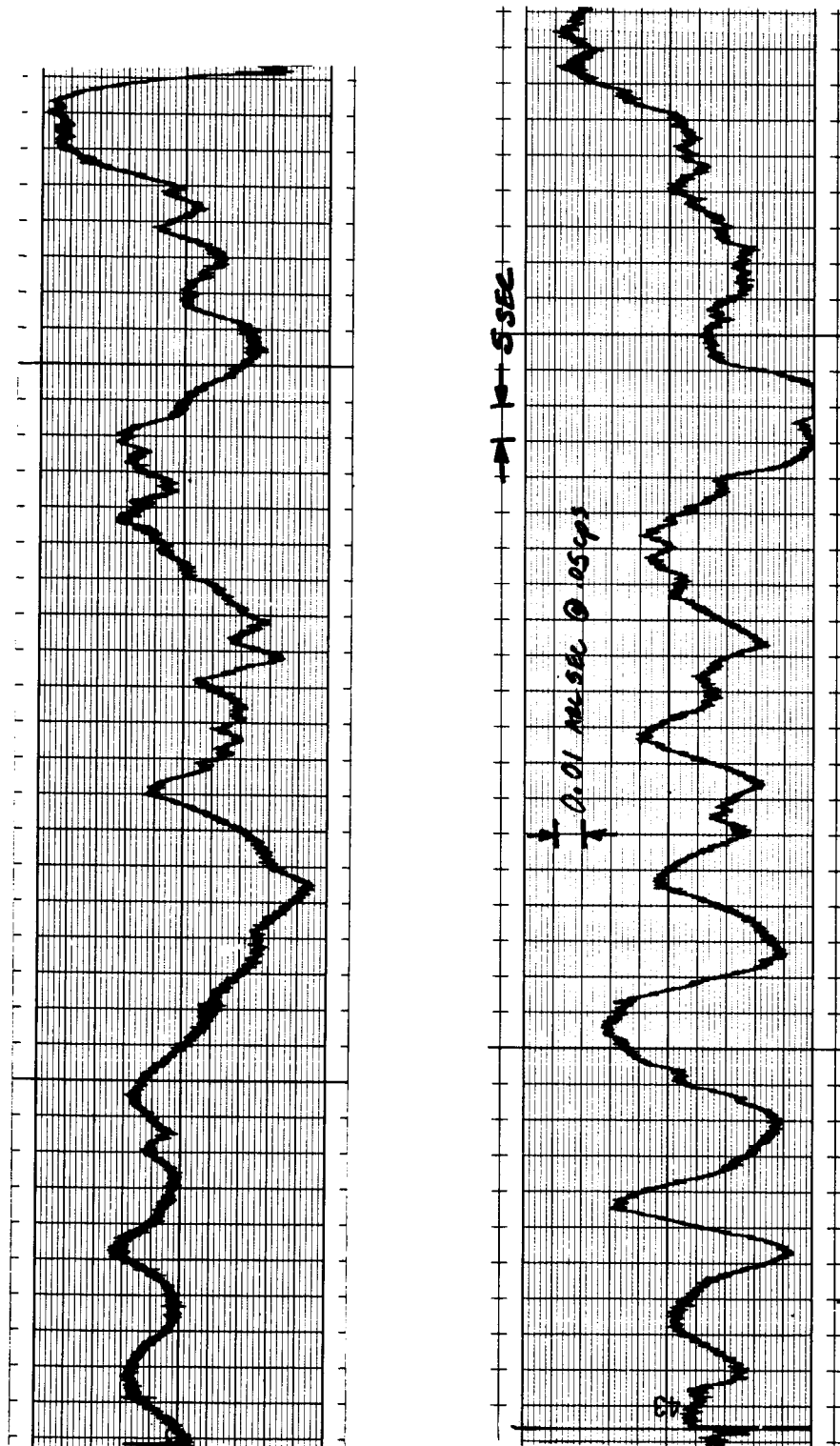
Figure 3.5.6 indicates what appears to be a wheel hunt induced by external mechanical means. The initial part of the trace shows seismic disturbances, measured by the monitor gyro with the table system in the level control mode (no gyro control). As a railroad train passed near the laboratory, the system was switched to gyro control to observe the degree to which a gyro-controlled system could eliminate this type of "cultural" noise. The resulting data illustrates an apparent improvement in the noise isolation performed by the gyro system except for burst periods of wheel hunting - conceivably excited by the train vibrations. To check this further, during a more quiet period, the table was tapped sharply while both the GI-V7 and the GI-T2 signals were recorded. The resulting oscillation, decaying exponentially, represents the classic wheel hunt signature. The maximum excursion measured by both gyros is approximately 0.2 arc-second.

To further analyze gyro noise phenomena, the output signal of the GI-V7 was next recorded at various chart speeds with the table clamped (see figure 3.5.7). The first trace illustrates the usual seismic input and does not reveal significant gyro noise. The next two tracings, taken at greater sensitivity and chart speed, indicate a 2.4 Hz wheel hunt with a peak excursion in the order of 0.013 arc-second referred to the input axis. This point is important since it illustrates that the effect of wheel hunt on a platform may be reduced by the gain of the gyro (at the wheel-hunt frequency). The wheel hunt measured here, incidentally, was with the GI-V7 connected to the same frequency source which seriously degraded the control gyro.

Next, noise measurements were made of the GI-T2 gyro along with the GI-V7 for comparison. See figure 3.5.8. This experiment also illustrates the amount of filtering which was required for reducing the GI-T2 noise to that of the GI-V7. Also of concern was the resolution capability of a gyro with a gain of one. The scaling, relative to the gyro input axis at the seismic frequencies, is set approximately equal. The GI-V7 noise, again, is in the order of 0.013 arc-second referred to the input axis. The GI-T2 excursions are in the order of 0.06 arc-second peak, and show a predominant 2-1/4 Hz wheel hunt frequency plus higher frequencies. A 60-cycle noise may be traceable to the 60-cycle GI-T2 heater control system that was especially constructed for this project.

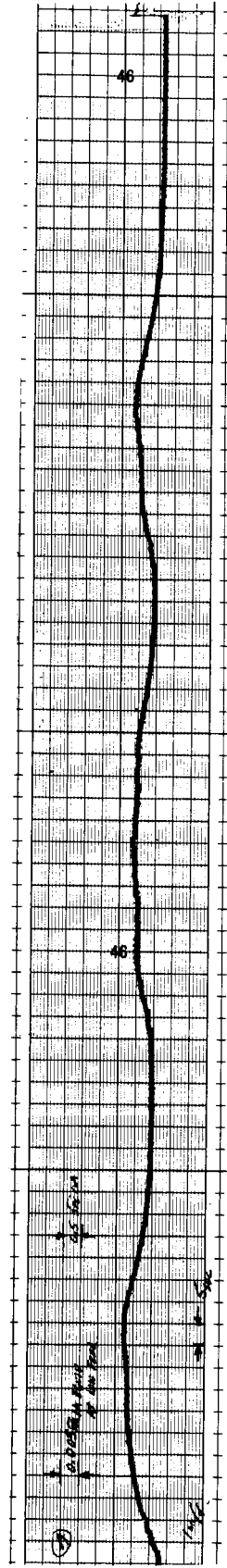
When the control loop is closed, the table angle variations, as measured by the V7 output, go from a relatively benign condition, to a 0.06 peak excursion characteristic of the control gyro wheel hunt.

Another source of short-term gyro noise which might go unnoticed for some applications, but is an important consideration in the control of stable pads within the fractional arc-second region, is thermal cycling of the heater control system. No obvious cycling of the GI-T2 control gyro was observed; however, thermal cycling of the GI-V7 gyro (using a standar SINS temperature controller) produced the tracing shown in Figure 3.5.9A. Figure 3.5.9B is the gyro signal after the temperature controller gain was reduced for better stability.

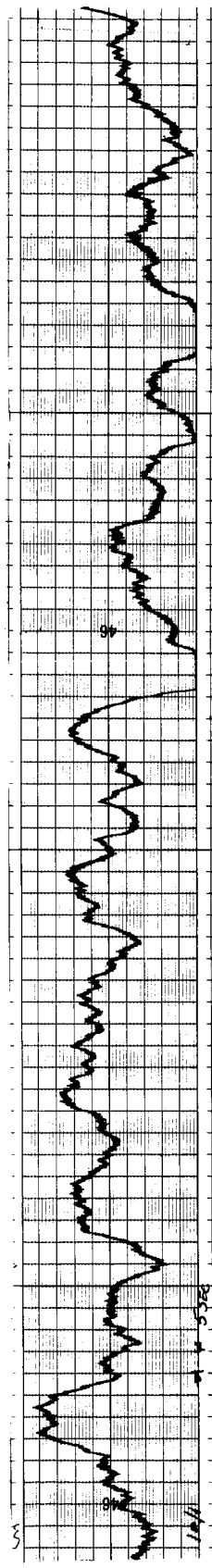


Sample Ground Motion, Measured with GI-V7 Gyro at NASA ERC

Figure 3.5.1



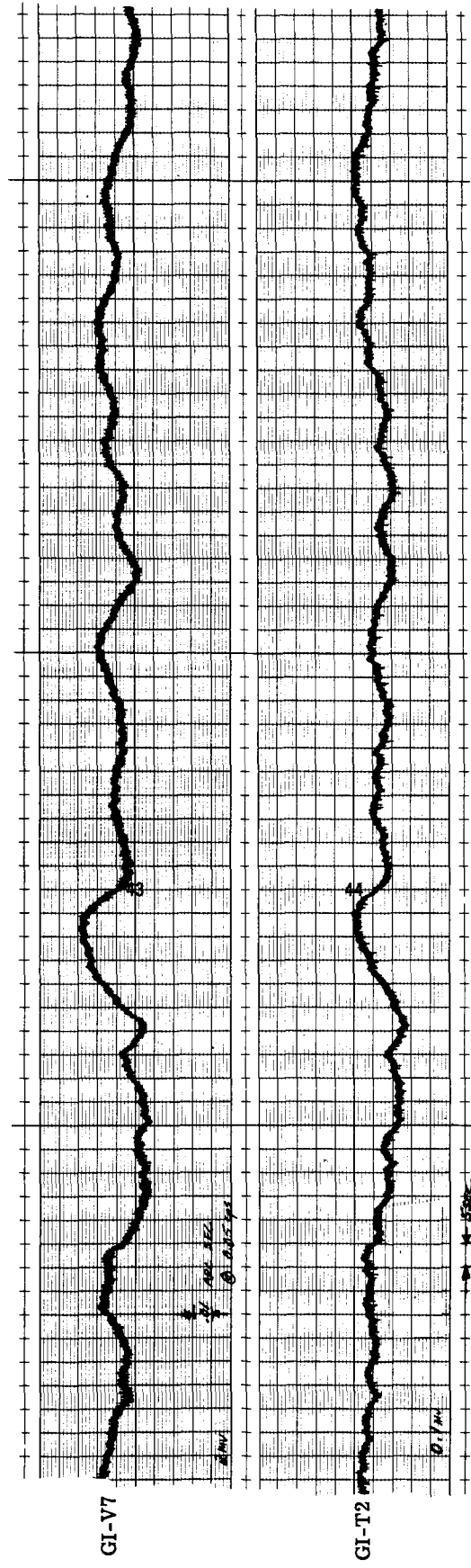
Wheel Off



Wheel On

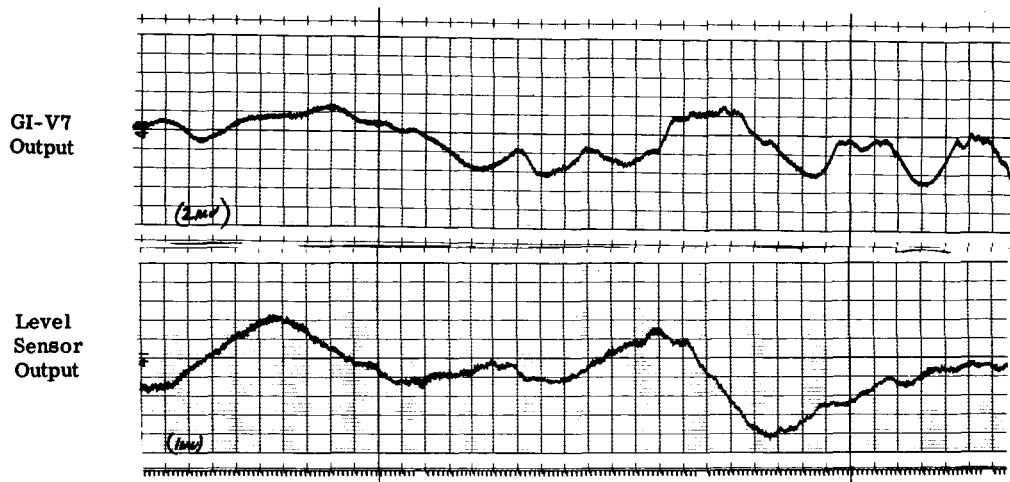
GI-V7 Output Signal Comparison Between
Wheel Off and Wheel On Condition
(Table Clamped)

Figure 3.5.2

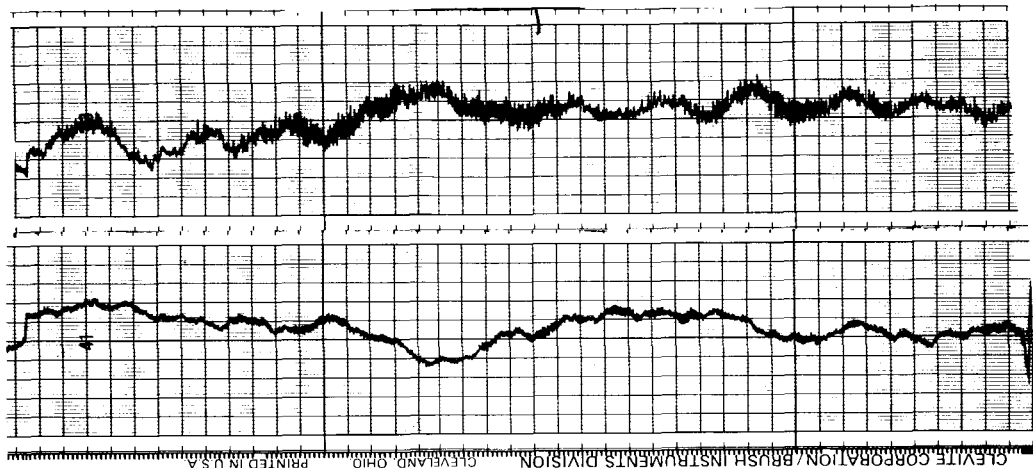


Comparison Between GI-V7 and GI-T2 Gyro Output Signals (Table Clamped)

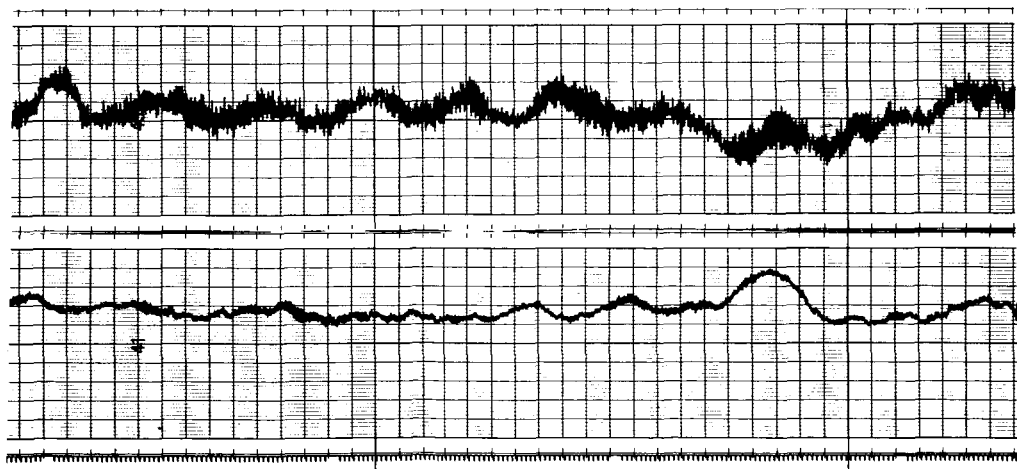
Figure 3.5.3



System Gain = 0



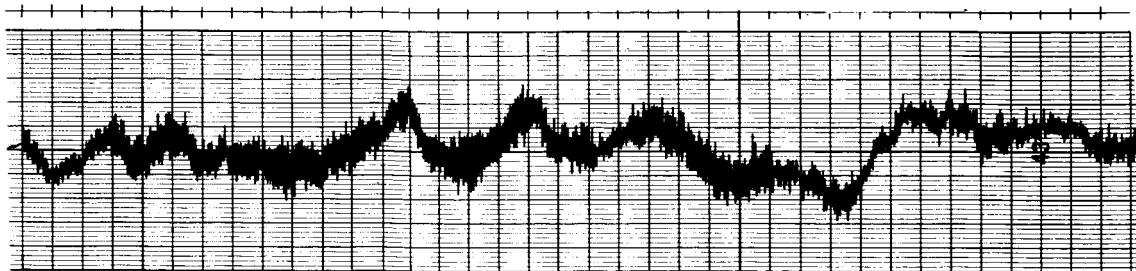
System Gain = 0.1



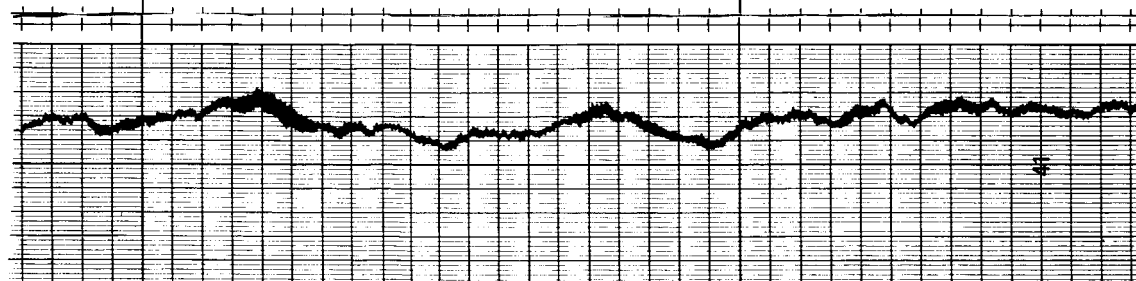
System Gain = 0.2

Figure 3.5.4.1

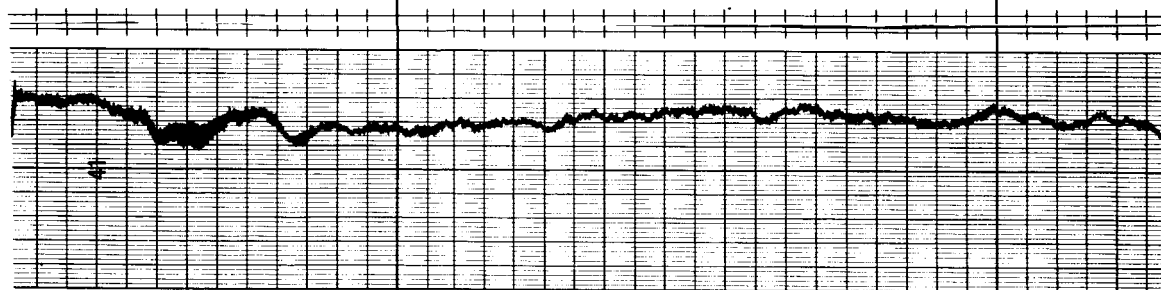
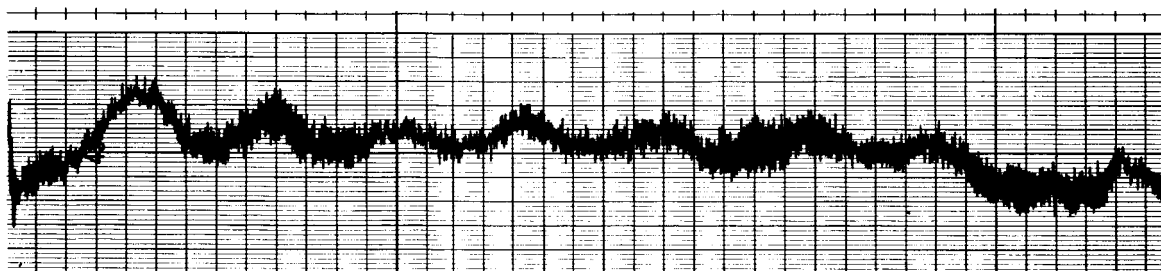
GI-V7
Gyro
Output



Level
Sensor
Output

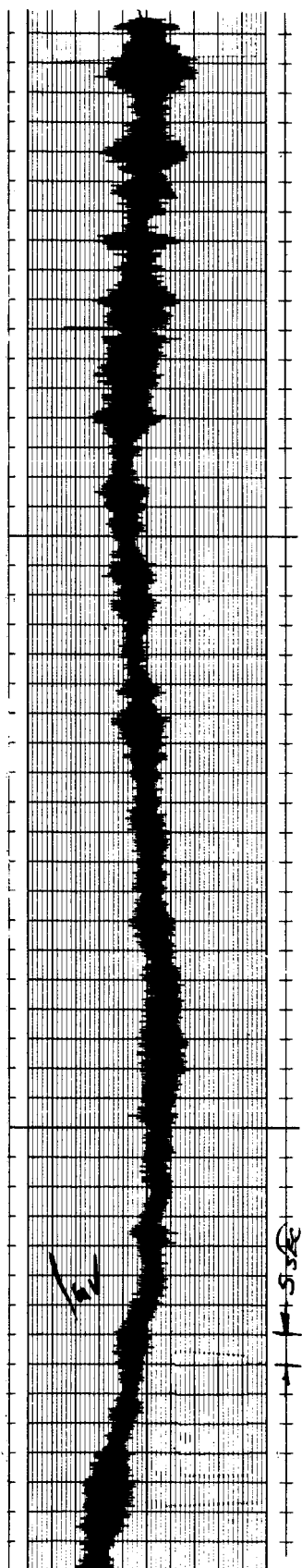


System Gain = 0.3

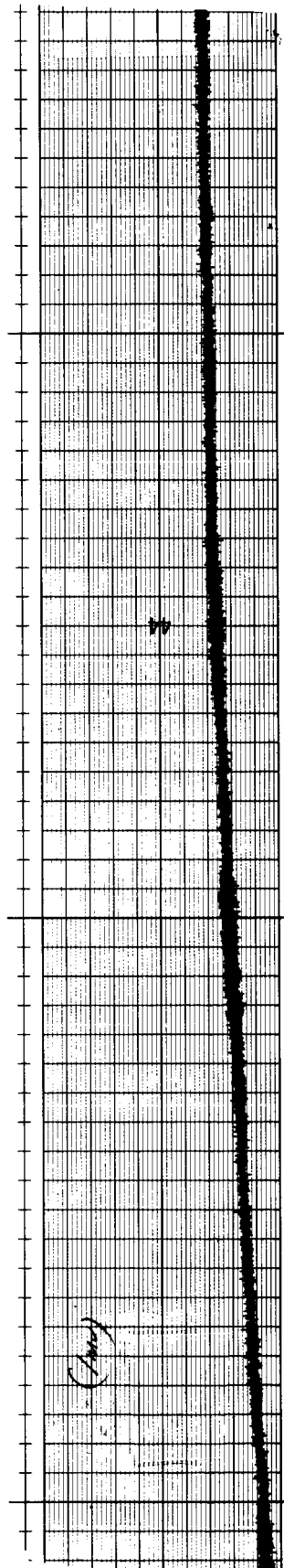


System Gain = 0.4

Figure 3.5.4.2



GI-T2 Output - Unstable Wheel Frequency



GI-T2 Output - Stable Wheel Frequency

Figure 3.5.5

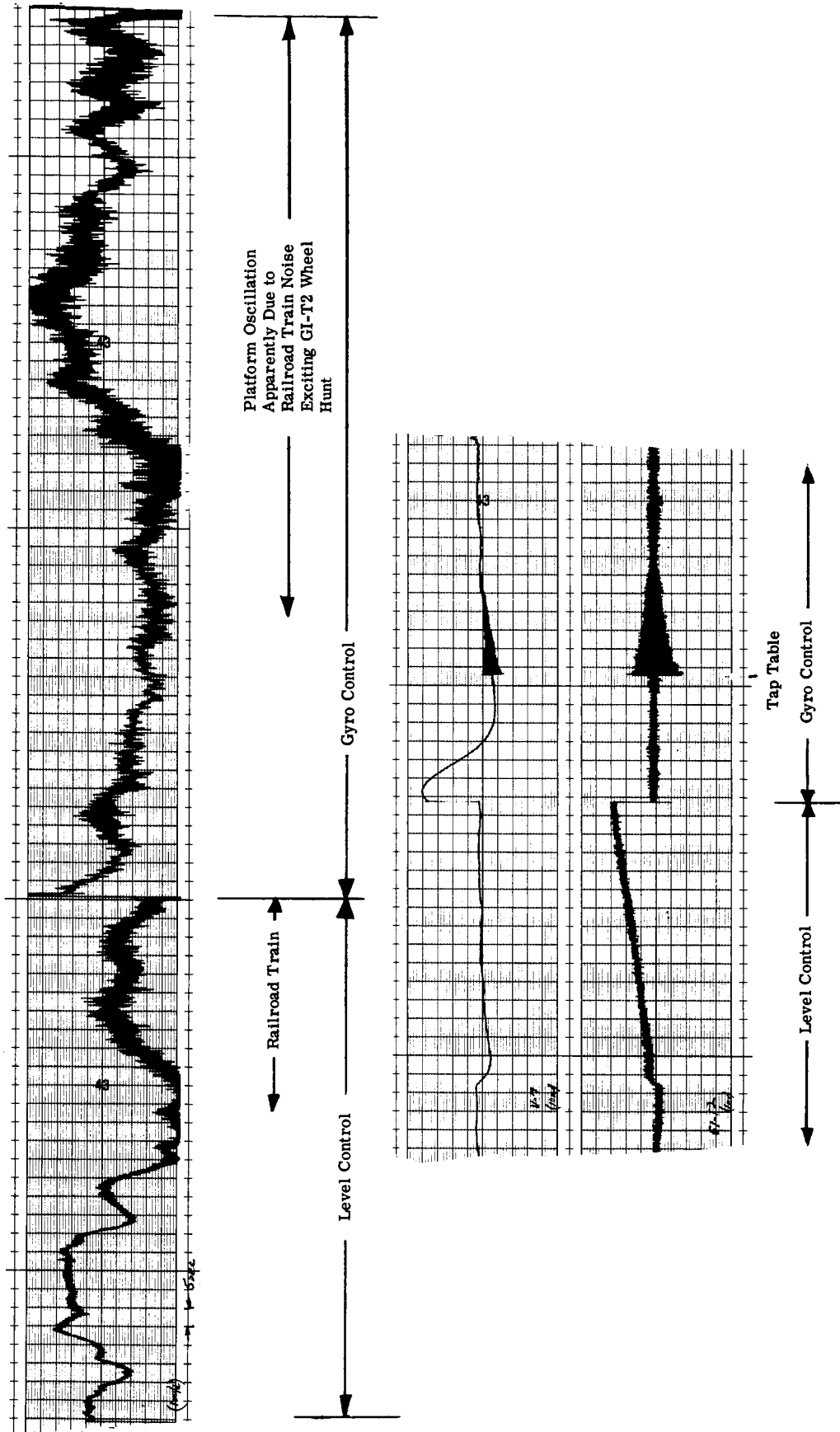


Figure 3.5.6

GI-V7 Noise Measurement

(Table Clamped)

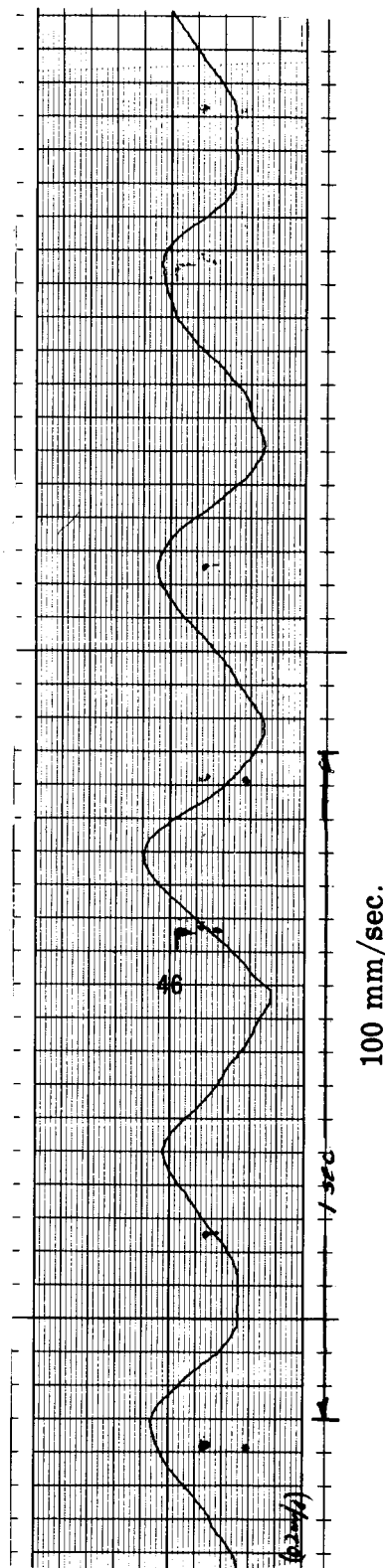
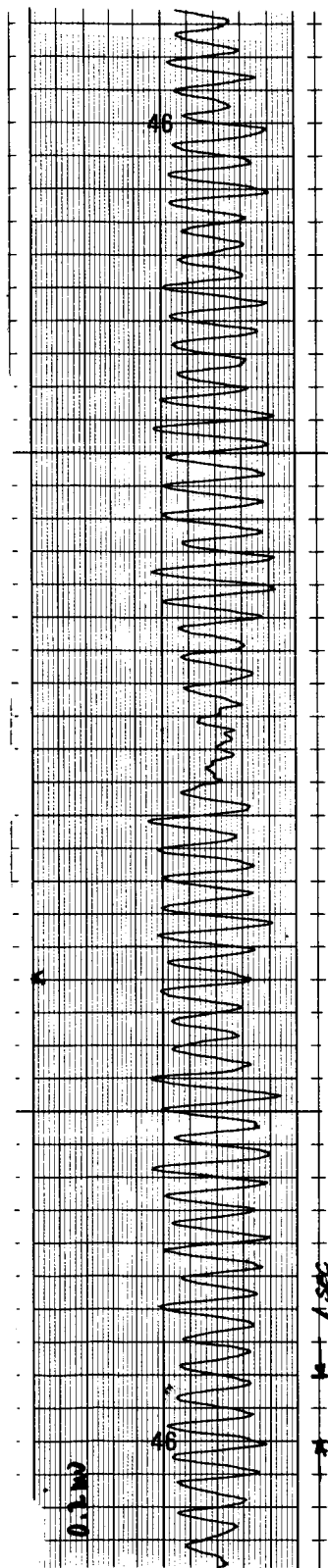
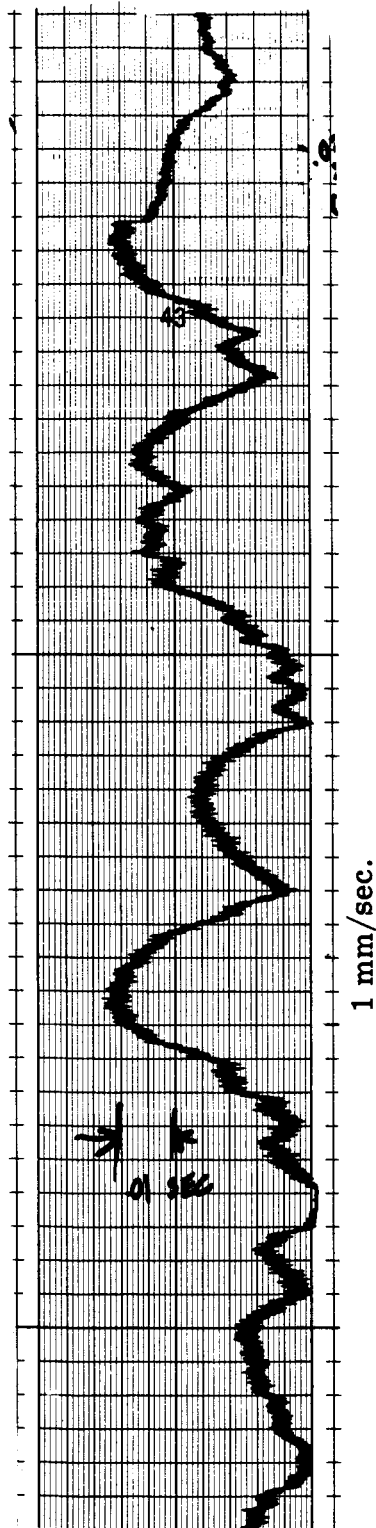


Figure 3.5.7

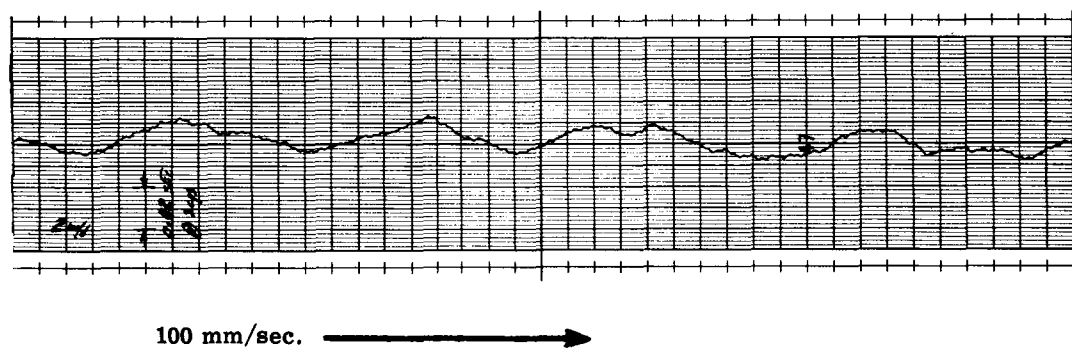
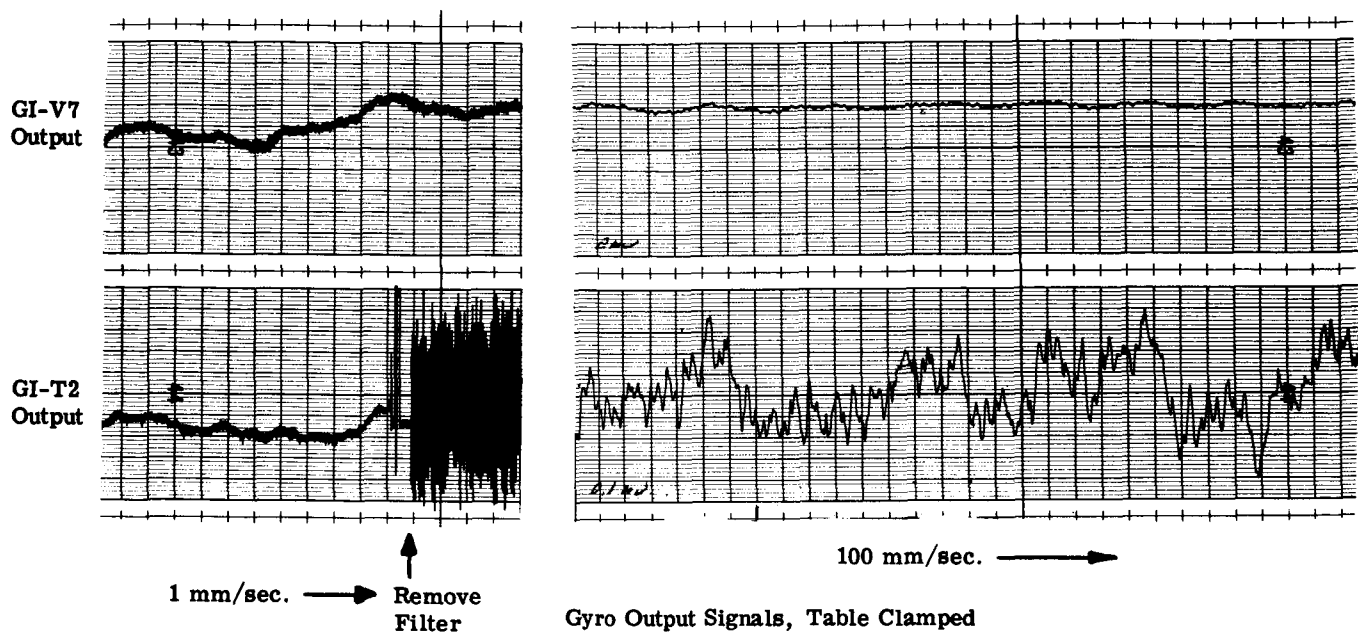
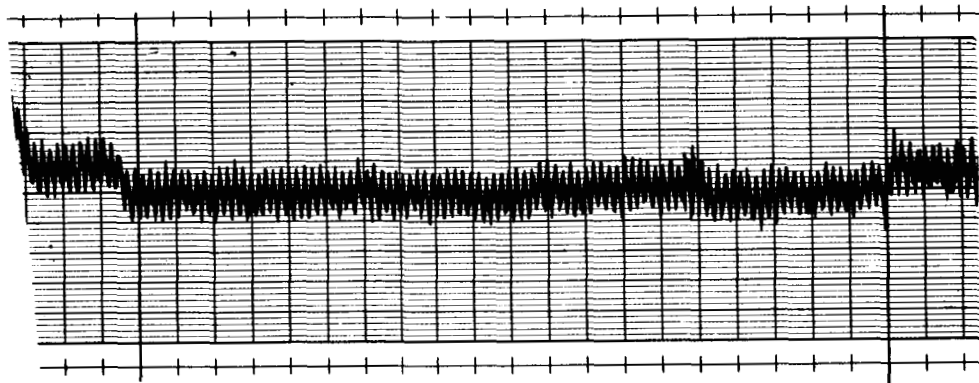
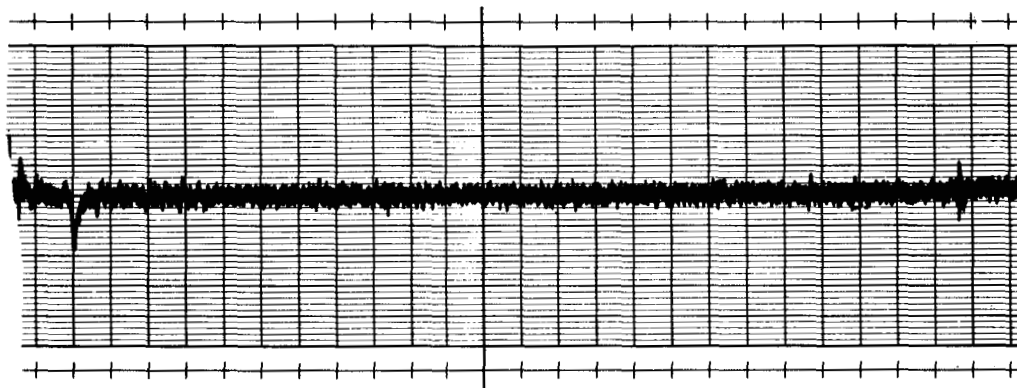


Figure 3.5.8 GI-V7 Output Signal, Gyro Control



A. GI-V7 Output Showing Temperature Cycling



B. GI-V7 Output with Stable Temperature Control

Figure 3.5.9

4.0 CONCLUSIONS AND RECOMMENDATIONS FOR FURTHER EFFORT

A marked improvement in the performance of the stabilized pad was obtained when the bandwidth of the control system was extended by adding a gyroscope to the control loop. Data obtained during these experiments indicates that when considering level data below 0.1 rad./sec. (the cutoff frequency of the level data filter), a 0.01 arc-second system is feasible. Without gyro control, the error is at least an order of magnitude larger.

The gyroscope, an almost ideal angular sensor for the system, exhibits two parameters which must be considered in the system design - drift and noise. Since a steady-state accelerometer signal in a combined gyro-accelerometer control system can be correctly interpreted as gyro drift, the system can be designed to be self-compensating, making it almost perfect at low frequencies. The use of a monitor gyro during these experiments focused attention on higher frequency disturbances (in particular, resulting from control gyro wheel hunt). This effect was significantly reduced by improving the short-term frequency stability of the wheel supply. However, further effort should be expended in the following areas:

1. Study the mechanism that couples the servo into the wheel spin-motor system. The data indicates that wheel hunt becomes more aggravated as servo gain is increased. This could be caused by gyro misalignment or by some higher order effect such as spin bearing torque modulation.
2. Investigate reducing the effect of wheel hunt by decreasing the radial sensitivity of the signal pickoff, increasing the output axis damping, or increasing gyro gain.
3. Decreasing wheel hunt by adding damping windings or other means for reducing the Q of the wheel spin motor system.

APPENDIX A

MONITOR GYRO CALIBRATION

GI-V7 Instrumentation

The GI-V7 instrumentation system consisted of a torque feedback loop with a manual drift correction adjustment (see figure). The capture loop contained an a-c preamplifier with quadrature rejection, a broadboard demodulator, and a high-quality operational amplifier. The a-c preamplifier gain was set at 187 to provide an output signal scaling of 10 mv./arc-sec. (about OA). The feedback gain was adjusted as low as possible while still maintaining a reasonable degree of gyro gimbal capture. A feedback amplifier gain of 0.1 was found to be quite satisfactory. The resulting loop gain was therefore 6770 dyne-cm./rad.

Calibration of the GI-V7 Gyro

The gain of an ideal single-degree-of-freedom rate integrating gyro, defined as the angular relationship between the output and input axes, varies with frequency. Therefore, to use a gyro to measure angular excursions of the platform, the gyro output data must be analyzed with respect to frequency and amplitude to obtain meaningful results.

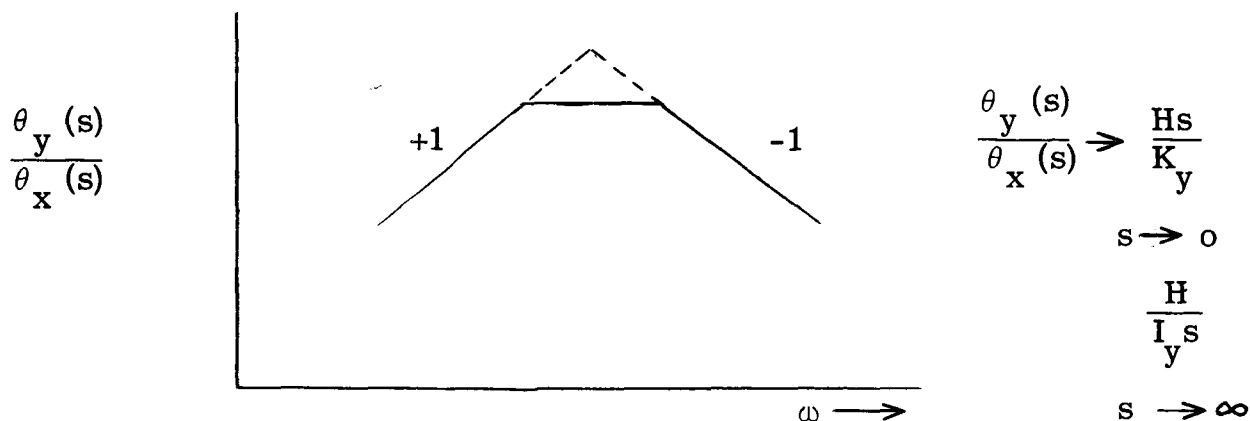
Consider first the frequency response of an ideal single-degree-of-freedom gyro which is described by the following

$$\frac{\theta_y(s)}{\theta_x(s)} = \frac{H}{I_y s^2 + C_y s + K_y}$$

where: θ = angle
 H = gyro angular momentum
 I = float assembly moment of inertia
 C = float-case damping
 K = total restraint term

x and y subscripts refer to the gyro input and output axes respectively

A plot of gyro gain vs. frequency for the ideal case will be of the form



A calibration curve of this form must be applied to the gyro data at each discrete frequency of interest so that the angular motions of the platform, measured by the gyro, will be correct.

Three methods of determining the response of the GI-V7 gyro were tried:

1. Applying calibrated torques about the output axis
2. Computing the response curve from known gyro parameters
3. Making a direct measurement of gyro response to inputs about the input axis.

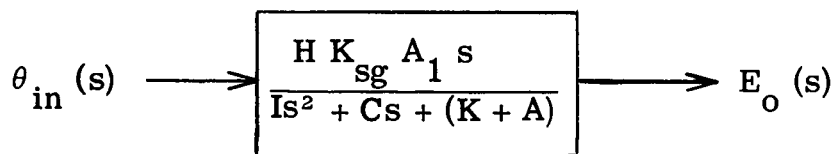
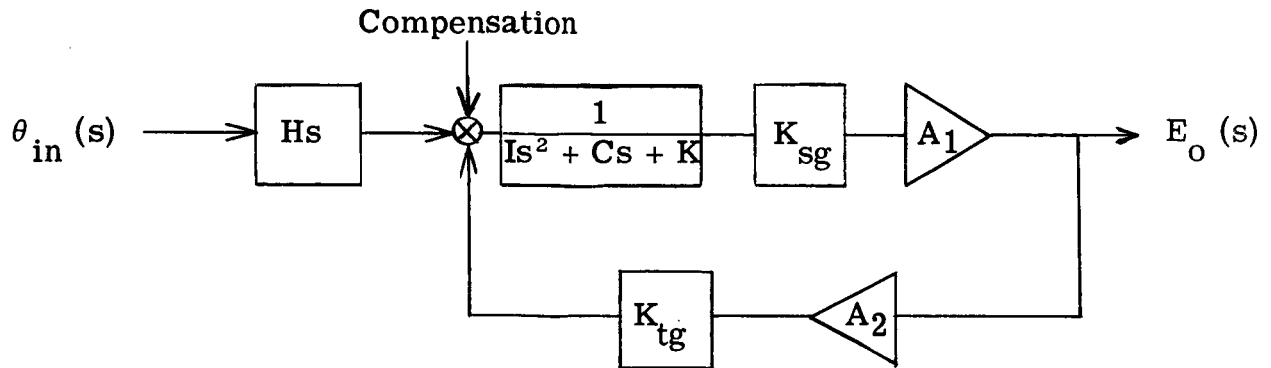
The first technique yielded poor results due to the input axis parameters associated with a non-ideal gyro. This method is analyzed below, but the data is excluded for this report.

The second technique, also an independent method of determining gyro response, yielded results in very close agreement with the data obtained by a direct measurement of gyro frequency response, the third method listed.

Analysis

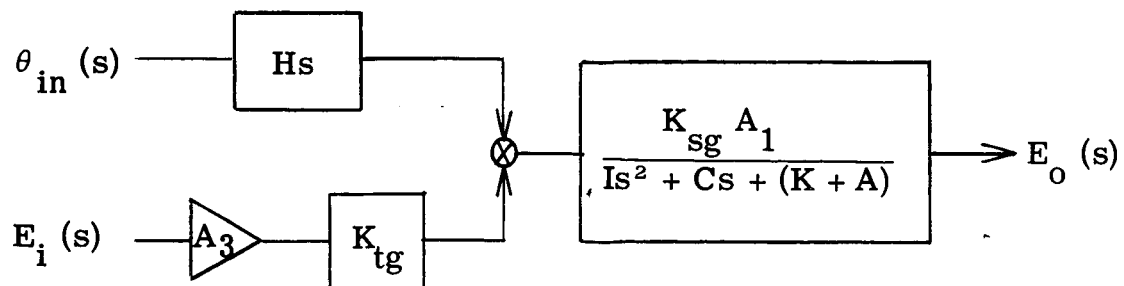
1. Calibration by output axis torquing:

A block diagram of gyro and instrumentation loop electronics may be shown as



where $A = \text{Loop Gain} = K_{tg} K_{sg} A_1 A_2$

The response of this system could be determined by introducing a sinusoidal driving signal into the torque feedback loop and then converting the second-order torque response data to that which would represent the response of the system to an angular input.



The $E_o(s)/\theta_{in}(s)$ response can be determined by multiplying the $E_o(s)/E_i(s)$ data by the quantity $(Hs/K_{tg}A_3)$. Both H and K_{tg} are known quite accurately so this method would seem to be a reasonable approach. As it turns out, however, when the x axis (input axis) parameters of the gyro are taken into consideration, as must be the case when dealing with real, non-ideal gyros, there is an error which will now be shown.

The output of the gyro and its associated instrumentation, when taking into consideration the second degree of freedom, is more precisely described by

$$\frac{E_o(s)}{\theta_x(s)} = K_{sg} A_1 \left[\frac{H C_x s^2 + H K_x s}{(I_x I_y) s^4 + (C_x I_y + I_x C_y) s^3 + (H^2 + K_x I_y + C_x C_y + K_y I_x) s^2 + (K_x C_y + C_x K_y) s + K_x K_y} \right]$$

$$= (H K_{sg} A_1) \left[\frac{C_x s^2 + K_x s}{\Delta} \right]$$

where the x and y subscripts refer to the gyro input and output axes respectively. This expression reduces to the perfect SDF gyro equation when all terms are divided by $K_x \rightarrow \infty$

Since the response of the TDF gyro to a torque about the output axis is

$$\frac{\theta_y(s)}{T_y(s)} = \frac{I_x s^2 + C_x s + K_x}{\Delta}$$

the response of the test system to the calibration procedure described is more precisely represented by

$$\frac{E_o(s)}{E_i(s)} = \frac{A_1 A_3 K_{tg} K_{sg} (I_x s^2 + C_x s + K_x)}{\Delta}$$

When data described by this expression is multiplied by $Hs/K_{tg}A_3$ the procedure for determining the $E_o(s)/\theta_x(s)$ response, the results will be of the form

$$\frac{E_o(s)}{\theta_x(s)} = (H K_{sg} A_1) \left[\frac{I_x s^3 + C_x s^2 + K_x}{\Delta} \right]$$

which differs from the real $(E_o(s)/\theta_x(s))$ response by the existence of the $I_x s^3$ term in the numerator or

$$\frac{E_o(s)}{\theta_x(s)} = \frac{E_o(s)}{\theta_x(s)} - \frac{I_x s^3 (H K_{sg} A_1)}{\Delta}$$

(angular) (meas- (error)
 ured)

A determination of the gyro gain vs. frequency by the application of output axis torques therefore requires that the magnitude of this error term be evaluated which, in turn, requires a determination of the gyro x and y parameters. Once these parameters are known, however, the gyro gain might as well be calculated directly from the transfer function equation which brings us to the second method to be considered.

2. Direct computation of gyro output using the exact expression for transfer function:

The following values have been determined for the GI-V7 gyro parameters:

$$\begin{aligned} I_x &= 2.15 \times 10^4 \text{ gm. -cm.}^2 \\ I_y &= 1.5 \times 10^4 \\ K_x &= 7.5 \times 10^8 \text{ dyne-cm. /rad.} \\ *K_y &= 7.55 \times 10^3 \\ H &= 9.2 \times 10^6 \text{ dyne-cm. -sec. /rad.} \\ C_x &= 3 \times 10^8 \\ C_y &= 5.9 \times 10^4 \end{aligned}$$

The K_y term is made up of three significant components: 1) gyro spring restraint existing within the gyro structure, 2) earth rate caging, and 3) electrical caging loop restraint. Typically the gyro spring restraint term is approximately 350 dyne-cm./rad. The earth caging term is computed by

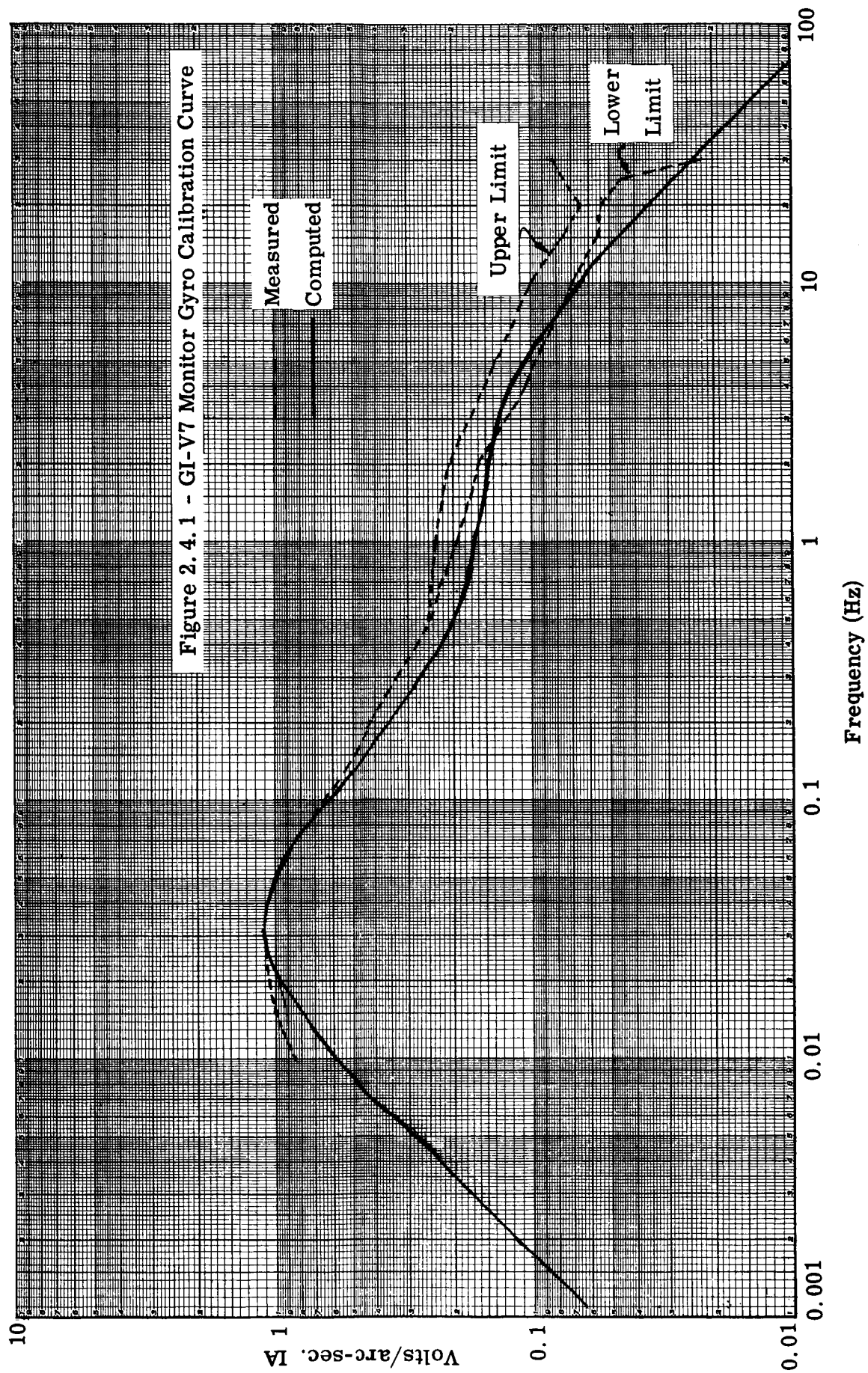
$$\begin{aligned} K_e &= H \omega_e \cos \lambda \\ &= 435 \text{ dyne-cm./rad.} \end{aligned}$$

The last term, that resulting from the electrical caging loop has been computed as $A = K_{tg} K_{sg} A_1 A_2 = 6770 \text{ dyne-cm./rad.}$

The results of this calibration are shown in figure 2.4.1 repeated here.

3. Direct measurement of GI-V7 gain

With the GI-V7 installed in the single-axis test model, the control servo was used to introduce known angular inputs to the gyro. The results are also shown in figure 2.4.1. Over certain frequencies, the results of these measurements agreed reasonably well with the computed values.



APPENDIX B

GI-T2-A

CHARACTERISTICS

Spin Bearing

Type

Hydrodynamic Gas Spin Bearing

Rotor

Angular Momentum

$1.84 \times 10^6 \text{ gm-cm}^2/\text{sec}$

Wheel Speed

24,000 RPM

Motor

Frequency

800 Hz \pm

Start Power

Peak Current/Phase

700 ma max. 650 ma typical

Voltage

55 rms

Power

40 watts max.

PF

0.52 typical

Running Power

Voltage

34 rms

Power

7.5 watts (max.)

PF

0.45

Phase Angle (B lags A)

$90^\circ \pm 5^\circ$

Float

Moments of Inertia

About Input Axis

$2,500 \text{ gm-cm}^2$

About Spin Axis

$2,830 \text{ gm-cm}^2$

About Output Axis

$2,070 \text{ gm-cm}^2$

Output Axis Bearing

Type

Magnetic Suspension

Excitation (sine wave)

Frequency	4,800 \pm 48 Hz
Voltage	
Tolerance	
Initial	3%
Short Term	0.5%
Long Term	1%
3-Year End Point	5%
Distortion	3% (max.)
Impedance (adjusted condition)	32.5 + j 51.6 ohms (each end)
Stiffness per pair (nominal)	
Axial	5 mgm/ μ in
Radial	80 mgm/ μ in
Rotational (about IA or SRA)	5.7 x 10 ⁸ dyne-cm/rad
Bottoming Circuit Resistor	100K ohms

Torquer

Type	Permanent Ring Magnet-Moving Coils	
	Coil A	Coil B
Torquer Scale Factor °/hr-ma	0.5	5.0
Max Torquing Rate °/hr	35 35	350 350
Stability	0.01% for 63 days	
Linearity	0.05%	
Maximum Current per Coil	70 ma continuous	
Polarity	Current from one end of coil through to other end of coil (not to center tap) would give an effective scale factor of 5.5°/hr-ma.	
Coil Resistance	100 ohms \pm 10% each side	
Temperature Sensitivity	0.01%/F°	

Pick Off

Excitation (sine Wave)

Frequency	4.800 ± 48 Hz
Voltage	5 rms
Tolerance	
Initial	3%
Short Term	0.5%
Long Term	1%
3-Year End Point	5%
Primary Impedance	
No External Circuit	53 + j434 ohms
Phase Angle	10°
Scale Factor	14 mv/mr ± 10%
Null Instability	1 sec (at operating temperature)
<u>Gain (H/C)</u>	1
<u>Characteristic Time I_o/C</u>	0.001 sec.

APPENDIX C
SUMMARY OF PROJECT ACTIVITY

August, 1967	Mechanical design of instrument package, gyro and level sensor mounting hardware, and draft shield.
September	Fabrication of hardware. Design of GI-V7 instrumentation, loop closure electronics, test console modifications.
October	Assembly and checkout of special electronics for the test console, completed test console modification.
November	Checkout of test console, evaluation of GI-V7 temperature control using electronic power supply for 400-cycle source (necessitated by absence of 400-cycle bench supply in NASA laboratory). Study and evaluation of monitor gyro calibration techniques.
December	Revision and reassembly of control system electronics at NASA/ERC. Assembly of mechanical components, installation of sensors and cabling. Modifications for adopting GI-T2 gyro to system. Construction of a special 60-cycle heater controller for GI-T2. Installed frequency doubler for clocking GI-T2 wheel supply from GI-V7 wheel voltage.
January, 1968	System checkout. Modified servo front end to reduce noise. Performed calibration of system. Started test runs. Closed loop frequency response and noise measurements for various servo compensation networks. Improved thermal stability of GI-V7 temperature controller. Completed level stability runs 1 through 5.
February	Placed floor angle monitors in position. Replaced GI-V7 microsyn supply. Further experimentation with gain settings and their effect on system noise and level stability. Made magnetic tape recording of system data and experimented with frequency spectrum analyzer. Completed level stability runs 6 through 12. Replaced operational amplifier in system.
March	Investigated erratic GI-T2 drift performance. Replaced GI-T2 gyro. Trouble not entirely cleared, checked for instability in electronics. Discontinued noise measurements using spectrum analyzer, resorted to direct recording technique at various chart speeds for separating frequency components. Identified predominant noise as GI-T2 wheel hunt. Performed further test to determine its cause and its effect on the system.
April	Reduced and analyzed data for final report. Commenced final report. Further study of gyro noise. Measurement of GI-V7 wheel hunt.

APPENDIX D

MAJOR EQUIPMENT USED

<u>ITEM</u>	<u>MANUFACTURER</u>	<u>MODEL</u>	<u>SERIAL NO.</u>
Gyro, Control	Nortronics	GI-T2	1
Gyro, Monitor	Nortronics	V-7	630
Level, Control	Ideal Aerosmith	DCTM-11	10806 (null meter) 10085 (sensor)
Level, Monitor	Ideal Aerosmith	DCTM-11	11643 (null meter) 11636 (sensor)
Level, Monitor	Taylor-Hobson	(Talyvel)	112/752-1014 (null meter) 112/753-1031 (sensor)
Level, (Floor Monitor	Ideal Aerosmith	R-DCTM-11	12365 (null meter) 12377 (sensor)
GI-T2 Wheel Supply	NH Research	SF379W	14517-W1
GI-T2 Microsyn Supply	NH Research	SF379M	14927-M1
V-7 Wheel Supply	Elin		119 (U.S. Govt. ID)
V-7 Microsyn Supply	Krohn-Hite		44 (U.S. Govt. ID)